Applied Energy 377 (2025) 124486

Contents lists available at ScienceDirect

Applied Energy

journal homepage: www.elsevier.com/locate/apenergy

A dynamic coordination of microgrids

Nsilulu T. Mbungu [a,b,*], Mukwanga W. Siti [b], Ramesh C. Bansal [c,e], Raj M. Naidoo [e], A. Elnady [c], Ali A. Adam Ismail [c,d], Ahmed G. Abokhali [c], Abdul-Kadir Hamid [f]

[a] Research Institute of Sciences and Engineering (RISE), University of Sharjah, Sharjah, United Arab Emirates
[b] Department of Electrical Engineering, Tshwane University of Technology, Pretoria, South Africa
[c] Department of Electrical Engineering, University of Sharjah, Sharjah, United Arab Emirates
[d] Department of Electrical Engineering, Omdurman Islamic University, Omdurman, Sudan, Africa
[e] Department of Electrical, Electronic and Computer Engineering, University of Pretoria, Pretoria, South Africa
[f] Department of Sustainable and Renewable Energy Engineering, College of Engineering, University of Sharjah, United Arab Emirates

GRAPHICAL ABSTRACT

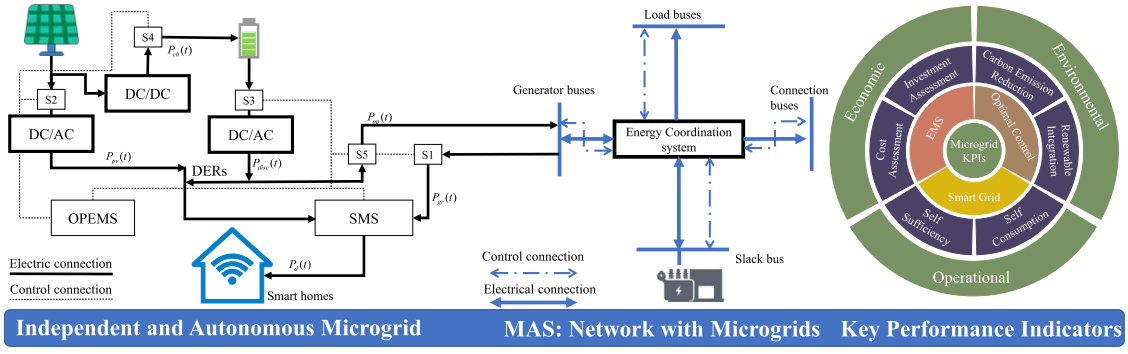

ARTICLE INFO

Keywords:
Key performance indicators
Energy management
Demand response
Model predictive control
Multi-agent system
Optimal control
Power flow analysis
Renewable energy
Smart grid
Voltage stability

ABSTRACT

Sustainable energy resource implementation has several advantages in terms of energy efficiency, reliability, and resilience. However, there are still challenges with the power quality in suitable energy balance and acceptable voltage levels in the electrical network. Therefore, this study presents novel energy coordination for implementing grid-tied microgrids, including photovoltaic and battery energy storage systems. Thus, multi-agent modelling based on system analysis is implemented to formulate the dynamic performance of independent, interconnected and autonomous microgrids. Three optimal control schemes, including open-loop, closed-loop and model predictive control, are combined with the optimal power flow algorithm to dynamically coordinate each independent agent and the entire microgrid. The system results demonstrate that, by combining these strategies with several smart homes, the dynamic coordination of microgrids brings various benefits, such as important economic, environmental and operation performance indicators, voltage stability, power loss minimisation and power-saving. The validation of the designed approaches is bench-marked within a 33-bus IEEE network in the residential sector. The developed intelligent coordination structures achieve significant energy savings ranging from 23.99% to 36.14% while maintaining suitable system voltage levels and minimising power loss. Besides, the developed dynamic coordination offers an adequate scalability framework for an effective microgrid implementation.

* Corresponding author at: Department of Electrical Engineering, Tshwane University of Technology, Pretoria, South Africa.
E-mail address: ntmbungu@ieee.org (N.T. Mbungu).

https://doi.org/10.1016/j.apenergy.2024.124486
Received 20 April 2024; Received in revised form 31 July 2024; Accepted 11 September 2024
Available online 21 October 2024

Nomenclature

Ha	Hours of autonomy of the BESS [hour]
A_{pv}	PV panel surface [m^2]
c_i	Carbon intensity
inf	Inflation rate
N	Computational time horizon
t, Δt	Sampling time and time variation [hour]
TE_{dp}	Total of energy produced from DEG
ϵ	Cost coefficient of the balance of the system
η	Number of principal component
η_{ch}, η_{dis}	Charging and discharging efficiencies of the BESS
η_{inv}, η_{pv}	Inverter and PV panel efficiencies
CB	Capacity of the BESS [kWh]
TE_{op}	Total opportunity energy
ϵ	Cost coefficient of the control system and design
ζ_c, ζ_d	Charging and discharging coefficients [1/kWh]
A	State matrix
B	Input matrix
C	Output matrix
$cost_x$	Energy cost from x component [kWh/Rand]
I_{pv}	Solar irradiation incident measured on the PV panel [kW/m^2]
Ic_λ	Installed capacity of component, λ [kWh or kW]
J	Objective function
N_c, N_p	Control and predicated horizons
P_{bat}	Power flow on the BESS
$p_{cap\lambda}$	Price of component, λ, [$/kWh or $/kW]
P_{ch}, P_{disc}	Power to charge and discharge the ESS [kW]
$P_{d.avrg}$	Hourly average power demand [kW]
P_{dc}	Power from the BESS to supply the load [kW]
P_d	Power demand
$p_{O\&M_\lambda}$, p_{Repl_λ}	$O\&M$ and replacement price [$/kWh or $/kW]
P_{op}	Opportunity power [kW]
P_{pv}	Generated power by the PV [kW]
$p_{r.ug}$, p_{der}	Real-time electricity pricing from the utility grid and DER [Rand]
P_{ug}	Power supplied by the UG [kW]
R	Reference signal
S, Q	Apparent and reactive powers [kVA], [kVAR]
u	Input vector/signal
V	Voltage [p.u]
x	State vector/signal
y	Output vector/signal
yr, N_{yr}	Number of year [year]

B&DCost	Annual Breakdown Cost
O&MCost	Annual Operation and Maintenance Cost
ACS	Annual Cost Savings
BESS	Battery Energy Storage System
BU	Battery Utilisation
CapCost	Capital Cost
CER	Carbon Emission Reduction
CL	Closed-Loop
COE	Cost of Energy
CS	Cost Savings
DEG	Distributed Energy Generation
DER	Distributed Energy Resource
DES	Distributed Energy Storage
DOD	Depth of Discharge
DR	Demand Response
Dr	Discount Rate
DSM	Demand Side Management
DSO	Distribution System Operator
ECS	Energy Coordination System
EMS	Energy Management System
EPBT	Energy Payback Time
ESS	Energy Storage System
IEEE	Institute of Electrical and Electronics Engineers
InvCost	Investment Cost
KPI	Key Performance Indicator
LCOE	Levelized Cost of Energy
MAS	Multi-Agent System
MPC	Model Predictive Control
NPV	Net Present Value
OL	Open-Loop
OPEMS	Optimal Energy Management System
OPF	Optimal Power Flow
PV	Photovoltaic
ReplCost	Annual Replacement Cost
RER	Renewable Energy Resource
RF	Renewable Fraction
ROI	Return on Investment
SalCost	Salvage Cost
SCR	Self-Consumption Ratio
SCRE	Self-Consumed Renewable Energy
SH	Smart Home
SMS	Smart Metering System
SOC	State of Charge
SOH	State of Health
SSR	Self-Sufficiency Ratio
TBC	Total Battery Capacity
TBEU	Total Battery Energy Used
TC	Total Cost of Project [$]
TCO_2E	Total CO_2 Emissions
TE_c	Total Energy Consumption [kWh]
TREP	Total Renewable Energy Production
UG	Utility Grid
VS	Voltage Stability

1. Introduction

The digitisation or modernisation of the energy system in the context of power flow is a technique that involves the energy efficiency of the electrical system. The dynamic modelling of microgrid applications is a platform that introduces different power coordination approaches in the power sector [1]. Those approaches establish several energy

efficiency schemes in the electrical network that mainly apply modern technologies. The commonly used concept to describe the digitisation or modernisation of the current electrical system is the smart grid [2,3]. The concept of intelligent grids brings an opportunity for real-time monitoring for both consumption and generation of power, bidirectional energy flow, and optimal integration of sustainable energy resources [4–6]. This opportunity leads to the overall improvement of the power system for all stakeholders, including end-users, distribution system operators (DSOs), distribution network operators, national or international power producers, and more [7].

The integration of energy resources (RERs) into the utility grid assists the DSO with better power flow efficiency when demand is increasing and power generation from conventional resources is unable to satisfy the total load demand [8]. In most scenarios of the energy management system (EMS), low-scale integration of RERs is implemented on the demand side [9] and large-scale integration on the distribution side for smart grid microgrid applications [10,11]. Therefore, the optimal sizing of distributed energy generation (DEG) technologies is critical for a suitable EMS scheme [12]. Through intelligent dynamic coordination, such as the EMS of a microgrid structure, the grid-tied RER brings more resilience and reliability into the power system behaviour of a given electrical network [13]. The intelligent dynamic coordination concept effectively relies on all benefits of microgrid development, deployment, and implementation, including autonomy, compatibility, cost-friendliness, efficiency, flexibility, peer-to-peer, scalability, and stability [7].

Aktas et al. [14] have implemented a dynamic energy management strategy to promote principal components of grid-tied microgrids based on RER. The implementation system manages the energy of a hybrid power storage system, ultra-capacitor and PV within a smart grid environment. The designed model assesses the dynamic change of the PV system. Thus, it is observed that the developed model improves the dynamic of energy management and system operations. Consumers get the opportunity to achieve optimal operational patterns, but it is challenging to identify the system modelling of the proposed dynamic algorithm. Besides, smart grid technologies offer novel approaches to control diverse end-user assets with an opportunity to dynamically model the electrical system [5,15]. Therefore, the consumers can effectively deal with the power flow into the electrical network by using the demand-side management (DSM) and demand response (DR) strategies [16,17], which introduce diverse energy price-based programs [18].

A dynamic energy management framework that combines a DR scheme with plug-in electric vehicles for residential rebound peaks is developed in [19]. The model is based on DSM using the features of intelligent metering. The optimal control strategy is modelled using the appliance timing dynamics controller, where the number of controllable devices and the price of electricity are suitably designed to assess the performance of the system. This conception can be regarded as a disadvantage of the proposed dynamic model when user-flexibility is required. In [20], a peer-to-peer power trading model is evaluated. This strategy is based on a near-optimal algorithm to optimise the system energy trading cost. It is observed that DSM plays an essential role in energy trading coordination [21]. Therefore, an alternating direction method of multiplier algorithm is developed for an effective decentralised energy market under peer-to-peer mode [22]. This strategy aims to create demand-side flexibility and give consumers an opportunity to mutually share energy. Ref. [23] also developed peer-to-peer energy trading in the framework of demand management with more focus on heater appliances. It has been observed that those energy trading schemes for the local community have a limited interaction on the DSO side as well as DEGs, even though the DR program was considered.

A performance assessment of different optimal control schemes is developed in [24] to create a full interaction on diverse DEGs and DSOs with more control action taken from the dynamic of the energy storage system (ESS). This is a real-world implementation of a smart home (SH) without any opportunity for the end-user, regardless of its technical advantages expressed by effectively handling the dynamic uncertainty of various DERs. In [25], energy coordination architecture for an SH is also presented without any opportunity through a combined power generation and energy consumption monitoring strategy for cost minimisation. This strategy-based communication applies ZigBee for the energy consumption and power line communication to coordinate RERs. Opportunity energy from the RERs and ESS is considered to be injected into the grid [26]. This is an occasion for the end-users to sell power to the DSO. Energy storage is regarded as one of the best options for an intelligent energy system to offer an opportunity framework [27]. This is because the ESS actively participates in decentralised electricity generation by creating a new type of power consumer called the prosumer that supplies and stores energy. In the EMS, the ESS is challenged by the total load hours for a given electrical system [28]. In [21], an MPC scheme is designed for the online energy market of the DSO that can coordinate ESS and power demand with wind power integration. The MPC strategy also provides a design scheme to effectively formulate a robust optimisation strategy based on feedback control that can effectively handle the system uncertainty from RERs [29].

In EMS, the robustness of the MPC implementation avoids the negative impact of the intrinsic uncertainties from DERs and secures the effectiveness of the system operation and a high penetration of RERs [30]. The dynamic modelling of the MPC-based optimal energy management scheme is implemented for hybrid electric vehicles in [31]. This is a new and improved MPC framework that is only limited to minimising the fuel consumption of plug-in hybrid electric buses, which coordinate the energy flow between electric vehicles. In [32], a combination of MPC with a decision tool and a multi-objective optimisation algorithm has been developed to formulate a novel EMS for a picogrid, a single household of less than 10 KVA demand [24]. This combined approach offers some trade-off solutions for microgrids while minimising the energy cost and carbon dioxide emissions of the entire system. Besides, the robustness of the MPC scheme provides an opportunity to handle various system uncertainties and forecast multiple variables. Ref. [33] proposes a combination of the MPC with reinforcement learning to design a novel reinforced MPC algorithm for building automation-based-EMS. This strategy lacks scalability due to the limitation of mathematical modelling but ensures continuous learning that can guarantee satisfaction and system automation. In [34], a distributed MPC is implemented to manage a grid-tied microgrid community with various distributed energy resources (DERs). The modelling strategy is formulated under a cooperation EMS to differ from the centralised strategy and resolve the complexity and difficulty of controlling a microgrid community without considering the opportunity of using ESS for the voltage stability of the entire system. Albeit, an optimal share of available power reciprocally that reduces operation cost and preserves the power balance between the DSO and all microgrids is guaranteed.

The power losses in the power system negatively affect the DSOs. The EMS has satisfied consumers by offering them an excellent energy cost profile, and the DSO by minimising the power losses in the entire network [10]. In [35], a novel intelligent energy system is developed to manage the energy system by reducing the cost and loss of power in the electrical grid. The model uses two-way energy and communication between the different components of a microgrid system. The model ensures the power balance between all active and passive distributed systems by integrating an intelligent storage system. The multi-agent system (MAS) is also used to minimise energy bills on the demand side, power transportation losses, and maximise grid service, especially during peak hours [15].

In [36], a MAS that constitutes a novel distributed event-based algorithm is designed for the EMS to maintain the power balance of the microgrid and improve the cycle life of the storage system. The EMS deals with the cost model of the power system within the

Table 1
Overview assessment of various applications for dynamic coordination of microgrids.

Ref.: Year	VS	EMS	OPF	DR	Op	MAS	Application
[30]: 2024	✗	✓	✗	✗	✓	✓	Game theory-based MPC for EMS with a large ESS
[40]: 2024	✗	✗	✗	✓	✗	✓	Peer-peer based on an optimal power sharing of ESS
[41]: 2024	✗	✗	✗	✓	✗	✗	Congestion coordination for a suitable energy market
[42]: 2023	✗	✓	✗	✗	✗	✓	Distributed EMS to coordinate multi-microgrids
[43]: 2023	✗	✗	✗	✓	✗	✓	Coordination of energy market and power system
[44]: 2022	✓	✓	✓	✗	✓	✗	Central control-based game theories for DSM
[45]: 2022	✓	✓	✓	✗	✗	✗	Coordinate large solar PV integration
[46]: 2022	✗	✗	✗	✗	✗	✓	Virtual power plant trading platform for DER market
[47]: 2022	✓	✗	✗	✗	✗	✗	Congestion management and cost minimisation
[48]: 2020	✓	✓	✓	✓	✗	✗	Coordination of an aggregation based-EMS
[49]: 2020	✗	✓	✗	✓	✓	✗	DR-day-ahead for optimal sizing and EMS of DERs
[50]: 2019	✗	✓	✗	✗	✗	✗	A framework for sizing and EMS various DERs
[51]: 2019	✓	✗	✓	✓	✗	✗	Voltage-load sensitivity scheme-based-DR
[14]: 2018	✓	✓	✗	✗	✓	✗	A dynamic EMS of grid-tied DES
This work	✓	✓	✓	✓	✓	✓	Apply system analysis to formulate optimal coordination of MAS with autonomous agents to guarantee cost reduction, energy savings and power loss minimisation of microgrids based-EMS and OPF.

VS: Voltage stability Op: Opportunity

active grid control strategy for intelligent grid applications [37,38]. An event-based mechanism is implemented to formulate a distributed optimisation strategy to coordinate different system agents [36]. The same conceptual approach based on an incentive mechanism to alleviate active power congestion is developed in [39]. The advantage of a multi-agent strategy is its ability to create an optimal decision from the ESS. This minimises operational costs and improves the overall system revenue by reducing power losses [7]. Table 1 compares the state-of-the-art methods of dynamic coordination of microgrids. This analysis details some relevant published works, including their pros and cons, to determine the absolute feasibility and uniqueness of this work.

The distributed energy system (DES) is essential in improving the EMS for both the DSO and the consumer [7,52]. This impact can be expressed in terms of energy efficiency of the entire system, network voltage stabilisation and energy loss reduction in the power lines [48]. From related works, a gap exists in implementing a DR-based real-time electricity pricing environment combined with an optimal power flow (OPF) to dynamically coordinate the energy flow in the electrical network. Besides, the optimal control of the energy management of microgrids is developed at the tertiary control layer with a high complexity level regarding the system modelling and its implementation in the MAS environment [7]. Besides, it has been observed that no one works, as presented in Table 1, has considered formulating some key performance indicators (KPIs) for microgrid implementation. Therefore, the novelty in this work is to develop dynamic microgrid coordination that consists of several smart homes (SHs) based on an optimal control scheme in a smart grid application. The system is validated with the 33-bus IEEE network, which offers scalability opportunities even in a residential application, as presented in [53–55]. The developed approach used the DR-price model to dynamically implement the power flow from the different components into the electrical network [56]. The design model applies the vision of control development and implementation of smart microgrids [7]. This invention is based on a tertiary control layer to formulate EMS of microgrids in the framework of linear and predictive techniques to harmonise a distributed control of MAS and ensure voltage stability and flexibility of grid-tied several autonomous SHs containing DERs. Thus, this dynamic microgrid modelling implements the tertiary control coordination based-EMS of a MAS through OPF under a DR technology. The contributions of this paper are as follows:

- Develop an intelligent approach to coordinating the power flow of microgrids. The method combines an optimal EMS with an OPF algorithm in the framework of the DR. Several independent and autonomous microgrids are coordinated within an electrical network for the effective operation of DSO. Therefore, the developed coordination strategy aims to dynamically manage microgrids and improve the system performance, including the acceptable voltage profile of the electrical network, optimal operation of grid-tied DERs and system efficiency.
- Apply the dynamic behaviour of the DES and DR real-time price schemes to develop three optimal control methods, including open-loop and closed-loop schemes and a quadratic model-based MPC. These control schemes are based on the tertiary control level of microgrids. They incorporate the EMS and OPF schemes to formulate a global performance index that can handle all the constraints of the electrical network and the variability of DERs.
- Design a flexible approach to a MAS constituting grid-tied microgrids, including solar PV and DES. Therefore, the developed dynamic coordination of microgrids is a multi-agent application where system modelling and analysis require a suitable combination framework between the designed optimal schemes of SHs and the OPF algorithm. Besides, the developed algorithm-based combination methods deliver a real-time and robust computational process for excellent system performance of an electrical power network with DER integration to guarantee acceptable voltage levels and offer suitable power saving while stabilising the power network with minimal power loss.
- Formulate KPIs based on economic viability, environmental impacts, and user satisfaction to assess the intrinsic dynamic behaviour of microgrids. The KPIs are developed within the energy trilemma perspective of microgrids, as presented in [7]. These are critical aspects that look at the economic, environmental and operational performances of dynamic modelling development for the effectiveness of microgrid coordination.

The remaining content of this work is divided as follows: Section 2 describes the network structure and DERs applied to the microgrid. Section 3 details the developed EMS. Section 4 presents results and discussions. Finally, a conclusion and perspectives for future research studies are highlighted in Section 5.

2. System description

2.1. Network configuration

The system configuration of the designed model is for residential applications and is illustrated in Fig. 1. The configuration model of this work used the electrical network presented in Ref. [57]. The network consists of a total of 33 buses, which are divided into three sections: buses 2, 3, and 4. For a comprehensive overview of the network, Table 2 provides a description based on all the buses in the system.

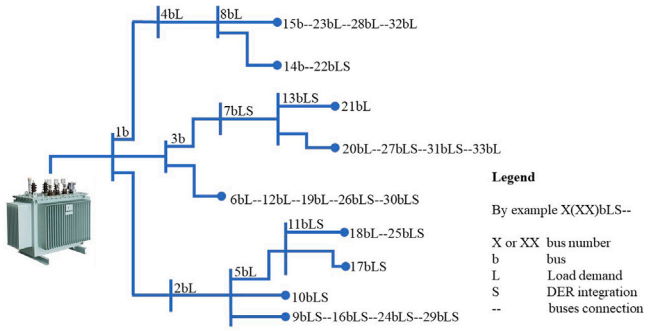

Fig. 1. Feeder: IEEE Network of 33 buses with 3 sectors.

Table 2
Electrical network identification.

Buses number	Type of buses	Load and DEG
1	Reference bus	–
2, 4, 5, 6, 8, 12, 18, 20, 21, 23, 28, 32 and 33	Load Bus	Only load
7, 9, 10, 11, 13, 16, 17, 22, 24, 25, 26, 27, 29, 30 and 31	Generator bus	Both load and DEG
3, 14, and 15	–	–

It is important to note that the generator buses in this configuration contain both load and DEGs.

As shown in Fig. 1 and detailed in Table 2, the DEGs comprise hybrid PV and BESS for each smart home. These components are connected to the grid at the generator buses. The utility grid functions as a backup to supply the total load demand when the DEG cannot generate sufficient power.

2.2. Distributed energy resources

In the electrical network depicted in Fig. 1, each generator bus employs a combination of PV panels and a BESS. Power is injected into the electrical grid from the BESS, primarily charged by energy produced from the PV system and also supplied to the load. Thus, the energy output from the PV system can be expressed as follows:

$$P_{pv}(t) = \eta_{pv} A_{pv} \sum_{t=1}^{N} I_{pv}(t) \tag{1}$$

where P_{pv} represents the power generated by the PV [kW], and t is the resolution [h]. The efficiency of the PV is denoted by ηpv. The surface area of the PV [m^2] is represented by A_{pv}. The computational time horizon, expressed in hours [h], is indicated by N. Lastly, I_{pv} signifies the hourly solar irradiance incident on the PV [kW/m^2].

The state of charge (SOC) of the battery describes the dynamic model of the BESS. Thus, $\forall t \in N \Leftrightarrow \Delta t = 1\text{h} \Rightarrow E_{bat} = \Delta t.P_{bat}$, with E_{bat} and P_{bat} are respective the energy and power flow on the BESS; thus, SOC can be formulated in function power flow on the battery as follows:

$$\text{SOC}(t+1) = \text{SOC}_i(t) + \zeta_c(t).\Delta t.P_{ch}(t) - \zeta_{dc}(t).\Delta t.P_{disc}(t) \tag{2}$$

where ζ_c, $\zeta_c(t) = \eta_{ch}(\eta_{inv}.\text{CB}(t))^{-1}$, is the charging coefficient [1/kWh], P_{ch} is the power to charge the battery [kW], ζ_{dc}, $\zeta_{dc}(t) = (\eta_{disc}.\eta_{inv}.\text{CB}(t))^{-1}$, is the discharging coefficient [1/kWh] and P_{disc} is the discharging power from the BESS [kW]. Both coefficients of the battery during the charging and discharging process are determined by the function of their respective efficiencies (η_{ch} and η_{disc}) of the energy storage, the inverter coefficient (η_{inv}) and the battery capacity (CB) [kWh], which is formulated as:

$$\text{CB}(t) = \frac{\text{Ha}.\Delta t.P_{d.avrg}}{\eta_{inv}.\eta_{disc}.\text{DOD}(t)} \tag{3}$$

where Ha is the autonomy of the BESS [h], $P_{d.avrg}$ is the average power demand for a given horizon N [kW/h], and DOD(t) is the depth of discharge of the ESS [50]. Thus, $\forall t \in \mathbb{N} \Rightarrow \text{DOD}(t) = 100 - \text{SOC}(t-1)$. Besides, in this work, the energy demand for each end-user is generated by the high-resolution energy demand model developed in [58].

3. Model development

The modelling process of the electrical network, depicted in Fig. 1, integrates the energy management of SHs into the electrical grid. This process involves the development of an isolated EMS, which requires coordination with the OPF of the power network.

3.1. Smart home description

The system model incorporates several distributed EMS, utilising a Smart Metering System (SMS) to function intelligibly within a grid environment. This EMS applies DR technology under a real-time electricity pricing scheme. As illustrated in Fig. 2 and detailed in Table 2, each Smart Home (SH) connected at every generator bus employs an optimal EMS (OPEMS). The OPEMS computes and coordinates system performance based on the DR scheme, optimally managing system switches such as S1, S2, S3, S4, and S5.

The control of the OPEMS is structured on an open or closed-loop model, ensuring it can supply optimal power to the smart home energy demand. Simultaneously, it must coordinate DERs and the utility grid (UG). This coordination aims to reduce power draw from the UG, maximise utilisation of DERs, and inject surplus power from the DER into the UG whenever possible. For the system described in Fig. 2, the vector $u(t)$ defines the system input vector. Thus, $\forall t \in \mathbb{N} \Rightarrow u(t) = [P_{pv_l}(t), P_{ug}(t), P_{dc_l}(t), P_{op}(t), P_{pv_b}(t)]^T$, with P_{pv_l} is the power flow from the PV to the load, P_{ug} is the power from the utility grid to supply the load, P_{dc_l} is the discharge power from the BESS to supply the consumer, P_{op} is the opportunity power from the DES which serves as the power to sell to the grid, and $P_{pv_b}(t)$ is the power from the PV to charge the battery which is also symbolised by $P_{ch}(t)$.

Therefore, considering the number of input signals $j = 5$, the power balances for the SH are formulated in Eqs. (4)–(6), as follows:

$$P_d(t) = \sum_{j=1}^{5} \left[\begin{bmatrix} 1 & 0 & 0 & 0 & 0 \\ 0 & 1 & 0 & 0 & 0 \\ 0 & 0 & 1 & 0 & 0 \\ 0 & 0 & 0 & 0 & 0 \\ 0 & 0 & 0 & 0 & 0 \end{bmatrix} u(t,j) \right] \tag{4}$$

with P_d is the power drawn on the demand side. In Eq. (4), this relation describes the first part of EMS on the SH system that supplies the load demand. The second part of the EMS is based on the energies that flow on the DERs. These also influence the load demand and the utility grid, and $\forall t \in N \Rightarrow P_{bat} = P_{disc}$ or $P_{bat} = P_{ch}$, where the charging energy is from the PV supply, as presented in Fig. 2. The energy flow during the charging process is formulated as:

$$P_{ch}(t) = P_{pv}(t) - P_d(t) \tag{5}$$

Eq. (5) $\Leftrightarrow \forall t \in N$, if $P_d(t) \leqslant P_{pv}(t) \Leftrightarrow P_{ch} = P_{pv_b}$, with P_{pv_b} is the power from the PV panel to charge the battery. Besides, Eq. (6) expressed the balance of the discharging process of the battery as follows:

$$P_{disc}(t) = P_{op}(t) + P_{dc_l}(t) \tag{6}$$

3.2. Energy management based-MPC

Dynamic modelling of the EMS can effectively be implemented using MPC strategy. The MPC scheme is formulated with three principal parts, including a predictive model, rolling optimisation and feedback correction. The objection function is the core of the predictive control that assists in predicting the future output response in the function of

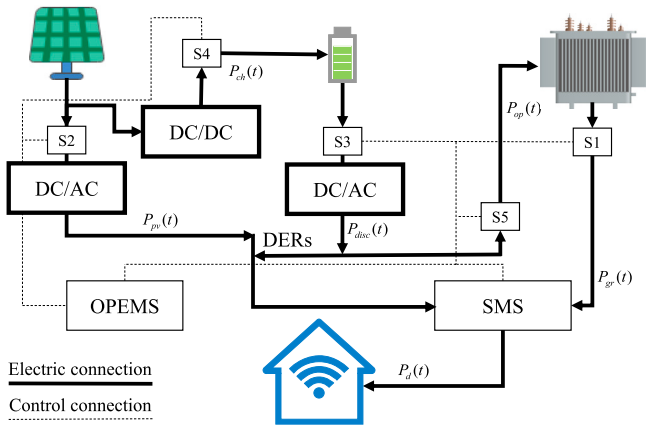

Fig. 2. An intelligent coordination of the smart home system.

the system state and the historical input of the system [40]. The MPC is also a robust and intelligent control technique that optimally handles several constraints and system uncertainty. These advantages make the MPC approach one of the most advanced and popular controllers to be used in various control engineering applications [7]. Fig. 3 presents the implementation formulation of the MPC strategy. An MPC design is model-based an optimal control method to optimally coordinate any dynamic system. Therefore, the dynamic scheme of the intelligent model developed in Fig. 2 can be implemented using an MPC approach. $\forall t \in \mathbb{N}$ if $k = t$, the control modelling of this dynamic system can be designed using a state-space model, as detailed in Eq. (7). In this work, the autonomous EMS for an individual agent is modelled with a quadratic MPC due to the formulation of its performance index.

$$\begin{bmatrix} x(t+1) \\ y(t) \end{bmatrix} = \begin{bmatrix} A & B \\ C & 0 \end{bmatrix} \begin{bmatrix} x(t) \\ u(t) \end{bmatrix} \tag{7}$$

where A, B, C, and $x(t)$ are the state matrix, the input matrix, the output matrix and the state vector. $u(t)$ and $y(t)$ denote the input and output variables. Thus, as presented in Fig. 2, the number of inputs $v = 5$. The system state vector x given Eq. (7) to be identified in the function of $u(t)$

MPC can be designed based on the costs of energy flow from each component, including the UT, PV, battery and the consumer. For instance, the cost of energy to pay the UG is defined as $Cost_{ug}(t+1) = Cost_{ug}(t) + p_{r.ug}(t)\Delta t P_{ug}(t)$. This formulation can effectively be used with all other components. Thus, Eq. (7) can be reduced as follows:

$$x_a(t+1) = I_{(v-1)}x_a(t) + B_a(t)u(t) \tag{8}$$

where $x_a(t) = [Cost_{ug}(t), Cost_{pv}(t), Cost_{bat}(t), Cost_l(t)]^T$, with $Cost_{pv}$, $Cost_{bat}$, and $Cost_l$ are the cost of energy flow on the PV, BESS, and on the demand side; $I_{(v-1)}$ is a 4×4 identity matrix with $v = 5$; $B_a(t)$ can be identified as a reduced input matrix which is formulated depending of each cost variable in $x_a(t)$ and $u(t)$ as:

$$B_a(t) = \Delta t \begin{bmatrix} 0 & p_{r.ug}(t) & 0 & 0 & 0 \\ p_{der}(t) & 0 & 0 & 0 & p_{der}(t) \\ 0 & 0 & p_{der}(t) & p_{der}(t) & p_{der}(t) \\ p_{der}(t) & p_{der}(t) & p_{der}(t) & 0 & 0 \end{bmatrix} \tag{9}$$

where p_{der} and $p_{r.ug}$ are the real-time energy prices from the DER and the UG. Thus, for the robustness of the system design, the state vector becomes the combination linear of SOC(t) from Eq. (2) in the function of Eqs. (5)–(6) and $x_a(t)$, and it is described as

$$[x(t)] = [\mathrm{SOC}(t), x_a(t)]^T \tag{10}$$

The state matrix of the system design is determined in function of Eq. (10) as:

$$A = I_v \tag{11}$$

with v is the rank of a matrix A, and I_v is a 5×5 identity matrix. Therefore, the input matrix, B, can be unidentified, based on Eqs. (7)–(11), as follows:

$$B(t) = \Delta t \left[\bar{\zeta}, B_a(t)\right]^T \tag{12}$$

with $\bar{\zeta}$ is the vec tor coefficient of the battery charging and discharging processes, $\bar{\zeta} = [0, 0, \zeta_{dc}, \zeta_{dc}, \zeta_c]$. The output matrix is determined in Eq. (13) based on Eqs. (7) to (12).

$$C = I_v \tag{13}$$

From Eq. (13), the output variable, $y(t)$, can be identified to be the same as the state vector, i.e. $y(t) = x(t)$. Thus, by considering the moving horizon presented in Fig. 3(b), the quadratic objective function of the MPC design presented in Fig. 3(a) is formulated as follows:

$$J(t) = \min \sum_{t=1}^{N_h} \sum_{j=1}^{N_c=t} (y(t|j) - R(t|j))(y(t|j) - R(t|j))^T \tag{14}$$

with $R(t)$ is the reference or target of the output signal, N_h is the predicted time horizon, $j = \Delta t$ is the control horizon sample with N_c the control horizon. The manipulated variable is then defined as

$$y(t) = Fx(t) + \Phi(t)u(t) \tag{15}$$

where $F(t) = \begin{bmatrix} CA & CA^2 & \cdots & CA^{N_h} \end{bmatrix}^T$, and

$\Phi(t) = \begin{bmatrix} CB(t) & 0 & \cdots & 0 \\ CAB(t) & CB(t) & & 0 \\ \vdots & \vdots & \ddots & \vdots \\ CA^{N_h-1}B(t) & CA^{N_h-2}B(t) & \cdots & CA^{N_h-N_c}B(t) \end{bmatrix}$. The MPC design for each SH is based on a quadratic performance index, while the open-loop and closed-loop schemes are linear models.

3.3. Smart network configuration

The configuration structure combines the OPEMS for each SH with the energy coordination system (ECS) of the entire electrical network. In Fig. 1, the system model between the network and the isolated SH, as described in Fig. 2, can be summarised in Fig. 4 by using a system analysis application. This structure derives from the network identification based on the type of buses from Table 2 to present the energy coordination network of the entire electrical system. The coordination of energy in the electrical grid, as proposed in Fig. 4, regardless of the hierarchical network of the system depicted in Fig. 1, operates in the EMS of all buses and their power flow, as shown in Fig. 1. Consider a given bus of the electrical network, such as the generator bus; the power flows in that ith-bus can be expressed as:

$$P_i = \sum_j \left[V_i V_j (G_{ij} cos(\theta_i - \theta_j) + B_{ij} sin(\theta_i - \theta_j))\right] \tag{16}$$

$$Q_i = \sum_j \left[V_i V_j (G_{ij} sin(\theta_i - \theta_j) + B_{ij} cos(\theta_i - \theta_j))\right] \tag{17}$$

with P_i and Q_i are the real and reactive power injected at the ith bus. V_i and θ_i are the voltage magnitude and phase angle at the ith bus. G_{ij} and B_{ij} are the conductance and susceptance between bus i and bus j. The sum is over all buses j in the system.

From Eqs. (16) and (17), the power balance of the apparent power at any time t in the AC system network can be written as follows:

$$S_i(t) = S_{gi}(t) - S_{li}(t) = P_i(t) + jQ_i(t) \tag{18}$$

where S_i, Q_i, and P_i are the measured apparent, reactive and active powers, i.e. $\forall t$ at a given bus i of the microgrid; $S_{gi}(t) = P_{gi}(t) + jQ_{gi}(t)$ and $S_{li}(t) = P_{li}(t) + jQ_{li}(t)$ are powers from the generator and load demand at the given bus i. The difference between buses depends on their type, whether load and DEG are connected or disconnected in the bus. For the stability of the electrical network, it is requested that the sum of Eq. (18) for all buses of the electrical network be zero.

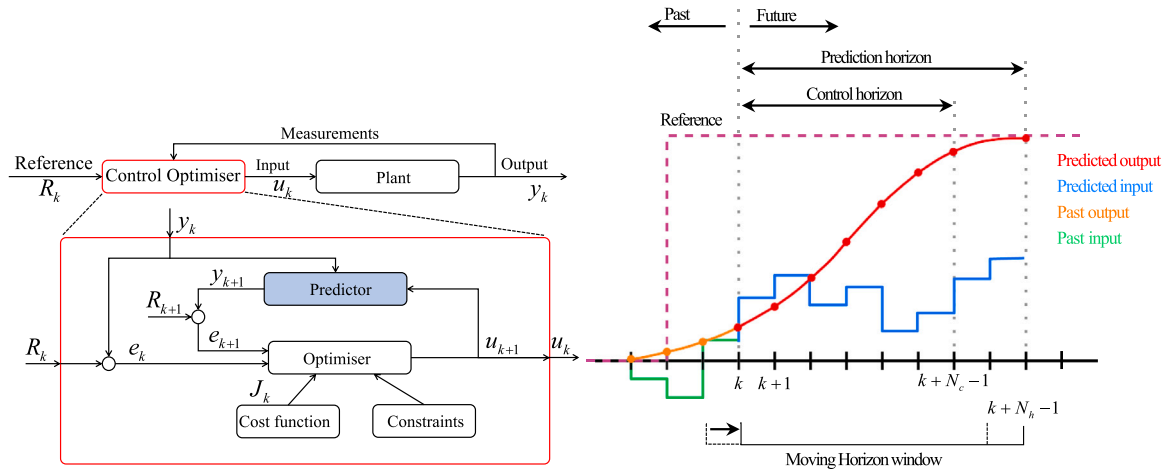

(a) Control loop. (b) Receding horizon.

Fig. 3. MPC: Implementation-based closed-loop optimal control scheme [59].

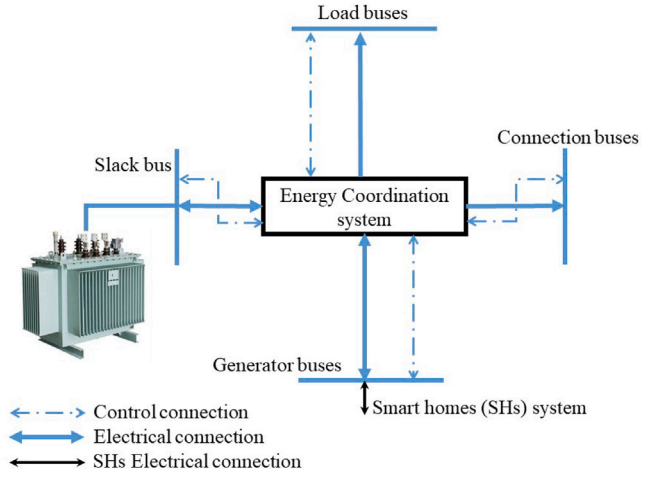

Fig. 4. A reduced dynamic MAS of grid-tied microgrids.

The possibility of respecting this hypothesis is to have the equilibrium between load and generator, expressed as:

$$\sum_{i=1}^{n} S_i = 0 \tag{19}$$

with n is the number of buses, which is 33, as presented in Fig. 1 and Table 2. Thus, $\forall t \in \mathbb{N} \Rightarrow \sum_{i=1}^{n} P_{gi} = \sum_{i=1}^{n} P_{li}$ and $\sum_{i=1}^{n} Q_{gi} = \sum_{i=1}^{n} Q_{li}$. The structure of this relation for the ideal power flow of the electrical system aims to have no power losses. When the SHs are not connected to any bus, which means that all generator buses in the system are off and there is only the load demand, Eq. (18) can be rewritten as follows:

$$S_{ug} = \sum_{i=1}^{n} S_{li} \tag{20}$$

In practice, a power loss may be associated with the relationship, as described in Eq. (20). Therefore, the energy coordination of the network, as illustrated in Fig. 4, aims to minimise the power loss and the reactive powers to enhance the system voltage. The reactive powers are determined by the function of the power factor of the entire electrical network, i.e. $\forall t \Rightarrow cost\varphi_i = 0.8$.

3.4. System performance index

The cost functions of the model are designed to evaluate the performance of each input system, considering their direct influence on the overall system behaviour. In the case of the SH system, illustrated in Fig. 2, the model's performance is determined by how well it coordinates the switching devices (S1, S2, S3, S4, and S5) to ensure an optimal power flow in the electrical system. When considering a specific SH of the electrical system, as presented in Section 3.1 and the energy cost in Eq. (8), if at $(t-1)$, it is assumed that the energy cost in the DERs is negligent, this can be formulated as:

$$Cost_{der}(t) = \Delta t.p_{der} \sum_{t=1}^{N} \left[P_{pv}(t) + P_{bat_s}(t) \right] \tag{21}$$

with $Cost_{der}$ is the energy cost of DERs based on the power from the PV and from the battery, including both the charging and discharging process, $P_{pv}(t) = P_{pv_l} + P_{pv_b}$ and $P_{bat_s}(t)$ is defined as the power supply from the battery. Thus, $\forall t \in \mathbb{N} \Rightarrow P_{bat_s}(t) = P_{dc_l}(t) + P_{op}(t)$.

The performance evaluation of the SH system is conducted under three different scenarios: open-loop, closed-loop and MPC schemes. Each scenario has its objective function to dynamically compute the microgrid. Eq. (21) is a function of power from the DERs, denoted by $P_{der}(t)$. Thus, $\forall t \in \mathbb{N} \Leftrightarrow P_{der}(t) = P_{pv_l} + P_{pv_b} + P_{dc_l}(t) + P_{op}(t)$. In the case of linear open-loop strategy, the objective function is determined by Eq. (22). This relation is the computational objective that combines the system dynamic of each SH component based on Fig. 2 and the integrated vision in Fig. 1. Furthermore, Eq. (22) captures the collective performance behaviour of the system, as described in Figs. 1–4.

$$J_{OL.b_i}(t) = \sum_{i=1}^{n_g} \sum_{t=1}^{N} \Delta t \left(p_{r.ug} P_{ug_{b_i}}(t) - p_{der} P_{der_{b_i}}(t) \right) \tag{22}$$

where $J_{OL.b_i}$ is the open-loop (OL) objection function of the system for each bus b_i; the same sub-index, b_i, is illustrated for each put variable $u(t)$, i.e. the PV, UG, discharging of battery, opportunity and charging process of the battery; n_g denotes the number of generator buses where the SHs are deployed. Thus, Eq. (22) can also be expressed as:

$$J_{SH.OL}(t) = \min J_{OL.b_i}(t) \tag{23}$$

Based on Eqs. (14) and (23), the performance index for the microgrid using MPC for the entire network is expressed in (24).

$$J_{SH.MPC}(t) = \min \sum_{i=1}^{n_g} J_{.b_i}(t) \tag{24}$$

with $J_{SH.MPC}$ is the MPC performance index for all SHs in the function of Eq. (14). The closed-loop performance index can be determined by

introducing a loop function in the cost signal of Eq. (22) to enable feedback. This concept is presented in Eq. (25). In this scheme, the introduction of j sampling is associated with the control horizon N_c to define the loop tactic. By incorporating feedback through the loop function, the closed-loop control strategy allows adjustments and optimisation based on the system performance throughout a control time horizon.

$$J_{SH.CL}(k) = \min \sum_{i=1}^{n_g} \sum_{k=1}^{N} \sum_{j=1}^{N_c=k} \Delta k(p_{r.ug} P_{ug.k_{j_{b_i}}}(k) - p_{der} P_{der.k_{j_{b_i}}}(k)) \tag{25}$$

with $J_{SH.CL}$ is the closed-loop (CL) objective function for all SHs in the system. It is necessary to note that the computation of open-loop and closed-loop schemes for this microgrid uses the dynamic of the energy storage system, as presented in Eq. (2), to perform an optimal control strategy.

In the open-loop process, the system has an initial state, SOC_0, at a specific starting time to influence the dynamic of the microgrid. However, it lacks the capability to compute time series data based on a variable input time horizon defined by N_c, as shown in Eq. (22). Besides, the closed-loop scheme enables a dynamic computation of time series data for the state variable by incorporating feedback and adjusting the system behaviour accordingly, as formulated in Eq. (25).

Fig. 4 describes the energy coordination of the entire electrical network. Assume that there is no SH-tied to the power network; the objective function of the network at a given time $t = k$ can be reformulated by using Eq. (20) as follows:

$$J_{EN}(k) = \min \sum_{i=1}^{n} P_i(k).p_{r.ug}.\Delta k \tag{26}$$

with J_{EN} is the objective function of the electrical network. Eq. (26) serves to compute the dynamic of an OPF control scheme for the energy coordination system of the developed electrical network, as summarised in Fig. 4. If it is hypothesised that open-loop and closed-loop contain a computational time horizon, N, Eq. (26) can be rewritten as Eqs. (27) and (28). These relations reflectively formulate the open-loop and closed-loop control schemes to dynamically compute the OPF algorithm.

$$J_{EN.OL}(t) = \min \sum_{i=1}^{n} \sum_{t=1}^{N} P_{b_i}(t).p_{r.ug}.\Delta t \tag{27}$$

$$J_{EN.CL}(t) = \min \sum_{i=1}^{n} \sum_{t=1}^{N} \sum_{j=1}^{N_c=t} P_{b_i.k_j}(t).p_{r.ug}.\Delta t \tag{28}$$

When considering the entire electrical system with the integration of DER through the SH systems, the objective function for the microgrid in both open-loop and closed-loop scenarios involves combining the cost functions of the SHs, Eq. (23) or (25), and the electrical network, Eq. (27) or (28). Therefore, their respective combined objective functions are formulated as follows:

$$J_{OL}(t) = J_{SH.OL}(t) + J_{EN.OL}(t) \tag{29}$$

$$J_{CL}(t) = J_{SH.CL}(t) + J_{EN.CL}(t) \tag{30}$$

where J_{OP} is the open-loop objective function of the entire system and J_{CL} is the performance index for the control scheme for closed-loop strategy.

Based on the quadratic model of the MPC scheme developed in (24) and the linear closed-loop scheme derived from Eqs. (25)–(30), the performance index of the MPC for the microgrid can be described in Eq. (31). This strategy is formulated by considering the moving horizon presented in Fig. 3(b).

$$J_{MPC}(t) = J_{SH.MPC}(t) + J_{EN.MPC}(t) \tag{31}$$

where J_{MPC} is the MPC objective function of the entire system, and $J_{EN.MPC}$ is the MPC objective function for the electrical network, which is based on the development perspective of Eqs. (14) and (28). For optimal computation, Eqs. (29)–(31) must be subjected to the system constraint, as detailed in 3.5.

3.5. System constraints

The system computation of the performance indexes, as detailed in Eqs. (29) and (30), is subjected to the same limits. The model implementation aims to compute the dynamic strategy of the energy storage based on the SOC approach, PV and utility grid through the use of DR as presented from Sections 3.1 to 3.4. The system constraint depends on the inequality limits of all the control variables [60]. Besides, SH for Eq. (31) is also subjected to state variables constraints in the function of Eq. (10). The minimum values of the input variables are set to zero. Therefore, for a given agent i, the maximum value of the input variable and the relevant components of the microgrid is a function of Eqs. (33)–(36).

$$u_i(t) \le u_{max_i} \tag{32}$$

$$P_{ug_i}(t) \le P_{d_{max_i}} \tag{33}$$

$$P_{pv_i}(t) \le P_{pv_{max_i}}, e.i, \forall t \Rightarrow P_{pv_{li}} + P_{pv_{bi}} = P_{pv_i} \tag{34}$$

$$P_{bat_i}(t) \le P_{ba_{max_i}}, e.i, \forall t \Rightarrow P_{ch_i} + P_{disc_i} = P_{bat_i} \tag{35}$$

$$P_{op_i}(t) \le P_{bat_{max_i}} \tag{36}$$

where u_{max_i}, $P_{d_{max_i}}$, $P_{pv_{max_i}}$ and $P_{bat_{max_i}}$ are the vector of the maximum value of each input signal, maximum power demand, maximum power from the PV and the maximum power flow from BESS, respectively, for the ith agent or bus. $\forall t \in \mathbb{N} \Rightarrow P_{ch_i}(t)P_{dsic_i}(t) = 0 \Leftrightarrow$ charging and discharging processes of the battery simultaneously are forbidden in the entire microgrid. This can also be expressed as

$$[\lambda_i, \lambda_i', \mu_i]^T u_i(t) = 0 \tag{37}$$

with λ_i and λ_i' represent the no-discharging process during the charging of the battery, respectively attached to P_{op_i} and $P_{pv_{bi}}$, and μ_i is the no-charging process while the battery is discharging. $\forall t \in \mathbb{N} \Leftrightarrow \lambda_i = [0,0,0,1,0]$, $\lambda_i' = [0,0,0,0,1]$, and $\mu_i = [0,0,1,0,0]$. Thus, λ_i and λ_i' also indicate that during the discharging process, P_{op_i} and $P_{pv_{bi}}$ are independent variables based on the dynamic performance of the entire systems. Besides, the SOC equality constraints also play an essential role in the computation of Eqs. (29)–(31). These are summarised by Eq. (38).

$$SOC_{min_i}(t) \le SOC_i(t) \le SOC_{max_i}(t) \tag{38}$$

where SOC_{min_i} and SOC_{max_i} are the minimum and maximum SOC_i of BESS. Eqs. (4) to (6) are considered the equality constraints of the system, as depicted in Fig. 2. These should be attached to each respective bus.

It is essential to note that, from Eqs. (33) and (38), the system details the constraints applied for a given SH. This approach can also be used for all intelligent demands in the system. For the entire electrical network, the system constraints must be subjected to the following:

$$S_{UG}(t) \ge \sum_{i=1}^{n} S_{d_i}(t) \tag{39}$$

where S_{d_i} is the apparent power demand at given bus i, S_{UG} is the maximum apparent power generated from the grid, which is different from the power supply–demand from the main grid to feed the end-user as shown in Eq. (33). Eq. (20) expresses the same maximum utility power, which is described in Eq. (39). The performance index aims to minimise the power loss on the electrical network. The voltage constraints are also considered to stabilise the system performance as designed in 3.4 for an excellent computational of an OPF algorithm. These constraints are expressed as:

$$V_{min_i}(t) \le V_i(t) \le V_{max_i}(t) \tag{40}$$

Table 3
KPIs for the coordination of microgrid.

	Performance indicators	Formulation	Eq.#
Economic	Cost of Energy (COE)	$COE = TC/(TE_c + TE_{op})$	(41)
	Cost Savings (CS)	$CS = (TE + TE_{opc} - E_{ug})p_{r.ug}$	(42)
	Energy Payback Time (EPBT)	$EPBT = TC/ACS$	(43)
	Levelized Cost of Energy (LCOE)	$LCOE = TC/TE_p$	(44)
	Net Present Value (NPV)	$NPV = \sum(ACS/(1+Dr)^{yr}) - TC$	(45)
	Return on Investment (ROI)	$ROI = (CS - TC)/TC$	(46)
Environ.	Carbon Emission Reduction (CER)	$CER = (TE_c + TE_{op} - E_{ug})c_i$	(47)
	Renewable Fraction (RF)	$RF = TREP/TE_c$	(48)
	Total CO_2 Emissions (TCO_2E)	$TCO_2E = E_{ug}c_i$	(49)
Operat.	Battery Utilisation (BU)	$BU = TBEU/TBC$	(50)
	Self-Consumption Ratio (SCR)	$SCR = SCRE/TREP$	(51)
	Self-Sufficiency Ratio (SSR)	$SSR = SCRE/TE_c$	(52)

Envrion.: Environmental Operat.: Operational

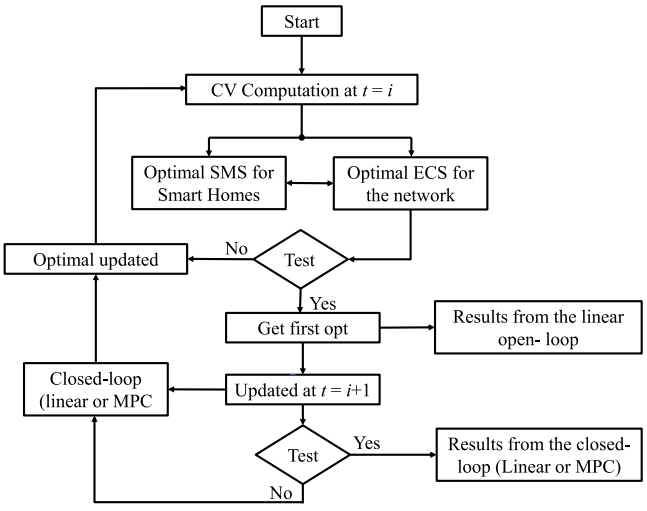

Fig. 5. System flowchart of the optimal control scheme.

where V_i, V_{min_i} and V_{max_i} are the voltage, minimum and maximum voltage at a given bus i.

The computational model solves the optimal strategies using a specific plan to compute the performance indexes, especially for open-loop and closed-loop methods with a different control process. This is observed in the control models formulated in Eqs. (29) and (30).

3.6. System flowchart and algorithm

Fig. 5 describes the flowchart of the developed model. The structure contains the control scheme for the linear open-loop, linear closed-loop and quadratic MPC models. At the start point, the system computes the control variable (CV) at time $t = 1$, which means all the input variables of the control scheme. These CVs are based on the entire network power from the solar PV, BESS with both the charging and discharging process, UG to load, and the opportunity power from DER to the power grid. It is important to note that on buses with no DER, the CV is the only power supply from the UG to the consumer for a given load bus i.

Based on the system flowchart, as described in Fig. 5, the computational algorithm is detailed as follows:

Algorithm Combining EMS and ECS (Open and closed-loop models)

A: Begin the computational process of the optimal control models
B: Set the time horizon and/or N_c for the optimisation process
C: System parameters updates at chosen $t = i$ with $i = [1..N]$
D: Measure the power from all components
E: $\forall t \in N$ if $t = i$, upgrade the network constraints
F: Compute both EMS and ECS using either Eq. (29) or (30) or (31)
G: Find the optimal value of the input signals
G.1: If not-optimal, redo steps A-G to reach the optimal value
H: Obtain the results for OL. Upgrade N_c at $t = i + 1$ for the CLs
I: Redo steps B-H for CL (linear and MPC) to reach N optimally
J: Obtain the optimal results for linear closed-loop or MPC
K: **end**

The described algorithm, from steps A to K, defines the process computation for both open and closed-loop schemes. The open loop is limited to step H, while the closed-loop scheme (linear and MPC) reaches up to step J.

3.7. Key performance indicators

A suitable coordination of microgrids should cover three principal KPIs, including economic, environmental and operational inductors. Table 3 summarises the most relevant KPIs of microgrids based on an EMS assessment for a given number of periods in years, yr, of the project. The economic KPIs are determined from Eqs. (41–46). Thus, TC represents the total cost of the project formulated in Eq. (53), TE_c is the total energy consumption of the system, TE_{op} is the total opportunity energy, E_{ug} is the energy consumption from the utility grid throughout the project life, TE_{dp} is the total of energy produced on the system from the DEG, ACS presents the annual cost savings expressed by $ACS=CS/yr$, and Dr is the discount rate. The environmental performance indicators are detailed in Eqs. (47–49), depending on the carbon intensity, c_i and the total renewable energy production (TREP). The operational KIPs depend on DEG for an effective operation of microgrids, as demonstrated in Eqs. (50–52), where TBEU is the total battery energy used, TBC represents the total battery capacity, and SCRE is the self-consumed renewable energy.

$$TC = CapCost + \sum_{yr=0}^{N_{yr}-1} [O\&MCost + ReplCost + B\&DCost](1+inf)^{yr} - SalCost \quad (53)$$

where CapCost is the capital cost of the project, N_{yr} represents the number of years to assess the project, O&MCost and ReplCost are, respectively, the annual operation and maintenance cost and the annual replacement cost for the principal components to implement microgrids, inf is the inflation rate, B&DCost is the annual breakdown cost, and SalCost salvage cost value is roughly considered to be 10 to 20% of the sum of the investment cost, $InvCost_\lambda$, of each principal component.

Thus, $\text{InvCost}_{\lambda} = Ic_{\lambda} p_{cap_{\lambda}}$, with Ic_{λ} and $p_{cap\lambda}$ represent the installed capacity and the price of component λ.

The total investment or the capital cost of the project, CapCost, is expressed as follows:

$$\text{CapCost} = (1 + \epsilon + \varepsilon) \sum_{\lambda=1}^{\eta} \text{InvCost}_{\lambda} \tag{54}$$

with η is the number of each principal component, λ, of the system that is directly attached to the investment cost of microgrids, ϵ presents the cost coefficient of the balance of microgrid for an effective installation, and ε is the cost coefficient of the control system and design. From Eq. (53), the annual costs are formulated as follows:

$$\text{O\&MCost} = \sum_{\lambda=1}^{\eta} Ic_{\lambda} p_{O\&M_{\lambda}} \tag{55}$$

$$\text{ReplCost} = \sum_{\lambda=1}^{\eta} \frac{Ic_{\lambda} p_{Repl_{\lambda}} \text{Dr}}{(1 + Dr)^{yr_{\lambda}} - 1} \tag{56}$$

$$\text{B\&DCost} = \sum_{\lambda=1}^{\eta} Ic_{\lambda} p_{Repl_{\lambda}} fr_{\lambda} \tag{57}$$

with $p_{O\&M_{\lambda}}$, $p_{Repl_{\lambda}}$ and fr_{λ} are, respectively, the annual operation and maintenance price replacement price and annual failure rate of component λ. Eq. (57) is attached to the replacement variables of each component.

4. Results and discussion

The system implementation of the described model is expressed in Section 3 and summarised, shown in Fig. 4. In this model, three principal scenarios of the energy coordination system are addressed in the framework of optimal power flow. These can be listed as follows:

- The first scenario computes the system with the generator buses. The modelling of the EMS is based on an open-loop computation strategy for each SH and the entire electrical network.
- The second model uses a closed-loop control strategy to implement the entire electrical system. The optimal computation scheme of the designed model is computed in real-time for both EMS, as presented in Fig. 2, and the energy coordination model, as depicted in Fig. 4.
- The last model uses the strategy developed in the third, based on the linear closed-loop model, to compute an optimal quadratic control based on MPC EMS. Thus, the control horizon, N_c, of the MPC scheme is set to be 5.

Besides, an isolated scenario to benchmark these three methods entails having a system that does not consider all generations based on the DEGs. This scenario only considers the impact of the load buses under optimal power flow coordination.

Table 4 gives the parameters for implementing the designed system, and the CB in each bus where the SH is integrated into the electrical network is designed using Eq. (3), with DOD = 0.1. It is a hypothesis that all initial values of the state of charge $\text{SOC}_{i_{int}}$ of the battery at each generator bus are set to be equalled. Table 5 describes the implementation parameters for KPIs assessment. These parameters have optimally been designed based on the Energy Market in South Africa. Therefore, the prices of energy, provided in Table 4, are converted into US Dollars for an effective evaluation of the economic performance, as presented in Table 3. Table 4 also provides capacities for the PV and BESS systems at bus 7. It is essential to notice that these capacities are sized to each bus in the function of maximum power demand. All these three scenarios are validated with $\text{SOC}_{i_{int}}$ =[0.4, 0.9], and $\text{SOC}_{i_{int}}$ = 0.7 is also considered to demonstrate the robustness of SH at bus 7. Furthermore, for an accurate assessment of the network, $P_{max_{ug_i}} = P_{max_{dc_{l_i}}} = P_{max_d}$, $P_{max_{pv_b}} = P_{max_{pv_{l_i}}} = P_{max_{pv}}$, and $P_{max_{op_i}} = P_{max_d}$.

Table 4
Implementation parameters.

Parameters	Values	Parameters	Values
$\eta_{i_{ch}}$	0.85	$[\text{SOC}_{i_{min}}, \text{SOC}_{i_{max}}]$	[0.4, 0.95]
$\eta_{i_{disc}}$	0.95	Ha	5 to 24
$\eta_{i_{inv}}$	0.92	N_h	24
pr_{gr} [ZAR/kWh]	1.25	N_c	[1 N_h]
pr_{rw} [ZAR/KWh]	0.65	3 × Converters_7 [kW]	20
CB_7 [kWh]	200	P_{pv_7} [kW]	22

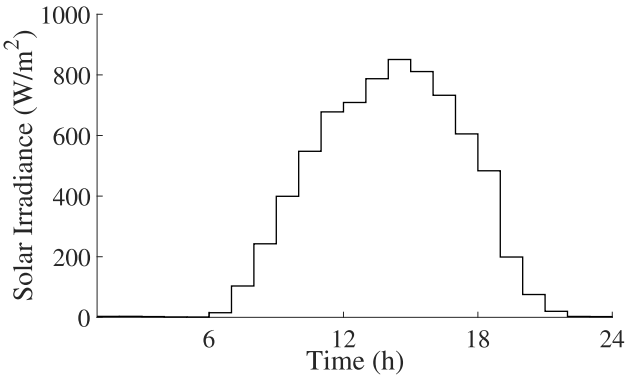

Fig. 6. Daily solar irradiance of the given electrical system.

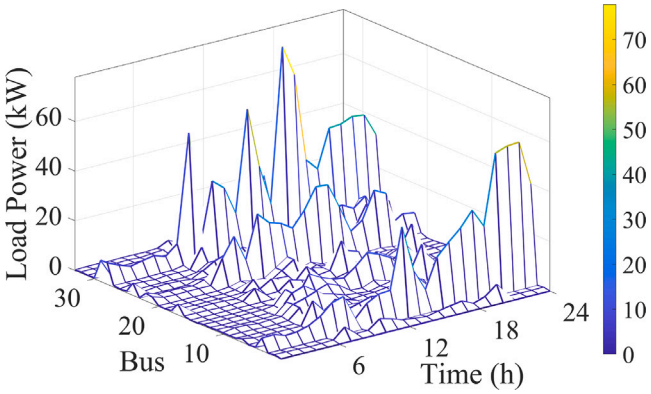

Fig. 7. The total load demand of the network.

4.1. Presentation of the results

The system design is tested using the energy demand and solar power forecasting model developed in [58]. Therefore, the high-resolution domestic model assists in structuring the hourly time series for energy demand. Besides, the sample irradiance profiles of solar in W/m^2 and a given day in May yield the system pattern. Thus, Fig. 6 depicts the solar radiation measured at a given panel. The hourly energy demand at all load buses is profiled through the maximum need for the residential sector-based IEEE 33-buses network, and it is presented in Fig. 7. This methodology uses the total dwelling power demand strategy. For instance, the PV system, energy storage and other computation parameters at bus 7 are expressed and can be devised based on Table 4. Their sizes depend on the maximum demand for each SH, as presented in Fig. 1 and explained in Fig. 2. Thus, the computational system uses the limitation structures developed in [60]. For instance, Ha is set at its minimal value of 5 h. However, the BESS applied in DERs can continuously discharge for 24 h or more [64].

Figs. 8 to 12 depict the optimal results for all control schemes based on intelligent energy coordination combined with several SH systems. Figs. 8–10 present the optimal results of the power-sharing scheme from

Table 5
Implementation assessment of KPIs [61–63].

Component (λ)	Investment price (p_{cap_λ})	Annual O&M price ($p_{O\&M_\lambda}$)	Replacement price (p_{Repl_λ})	Annual failure rate (fr_λ)	Lifespan (yr_λ)
PV System	300 [$/kW]	10 [$/kW]	200 [$/kW]	0.05%	25
ESS	226.26 [$/kWh]	10 [$/kWh]	140 [$/kWh]	4%	10
3×Converters	150 [$/kW]	5 [$/kW]	100 [$/kW]	2.5%	15
c_i: 0.6569395 kg CO_2/kWh		Dr=inf: 0.0527	ϵ: 0.25	ε: 0.125	

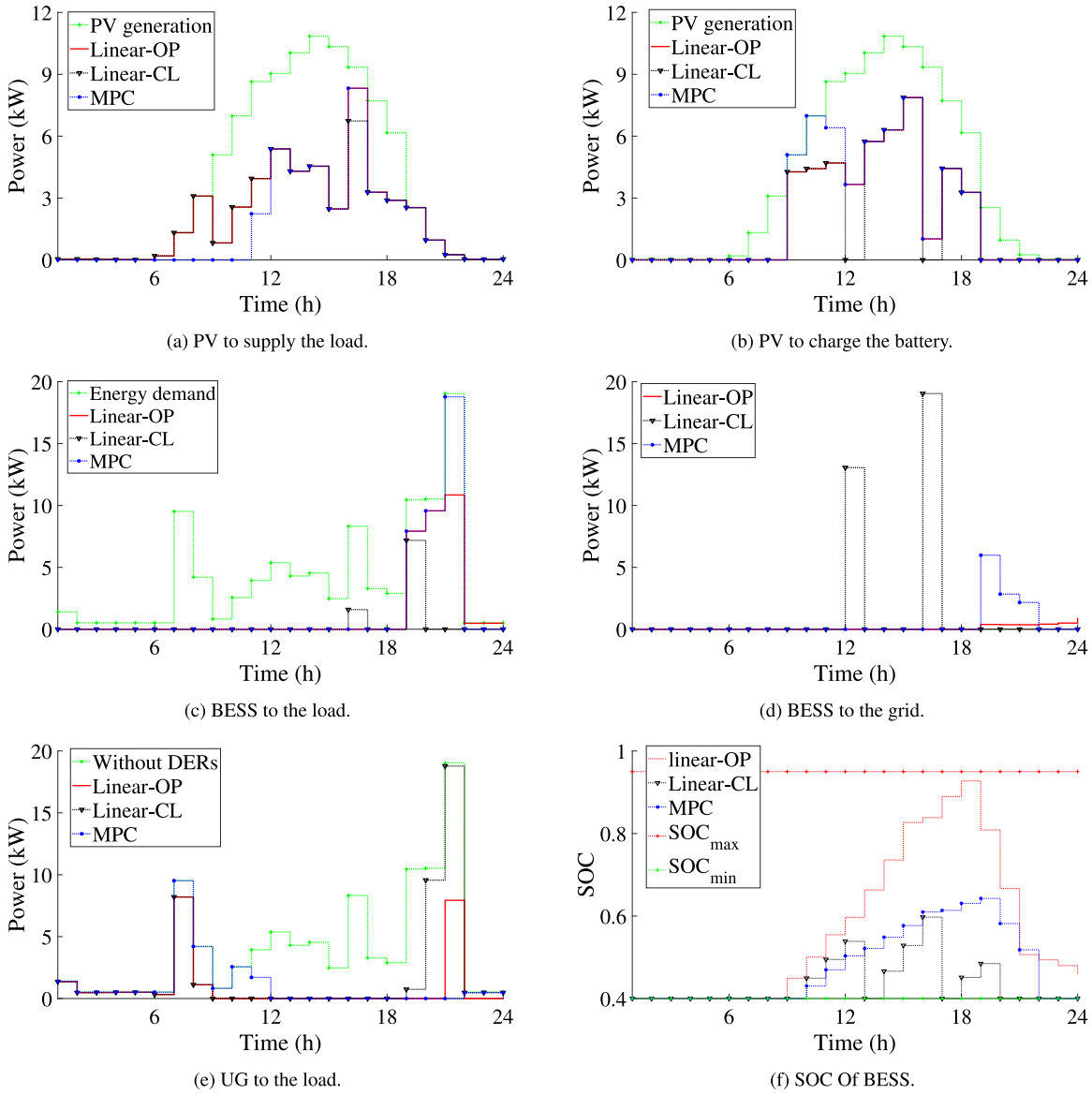

(a) PV to supply the load.
(b) PV to charge the battery.
(c) BESS to the load.
(d) BESS to the grid.
(e) UG to the load.
(f) SOC Of BESS.

Fig. 8. Optimum coordination of microgrid at bus 7, with initial SOC_{int} = 0.4.

DERs into a given SH with three different values of SOC_{int} = [0.4, 0.7, 0.9]. The power flow pattern is considered at bus 7 [57]. It should be important to note that the results in Fig. 8 are implemented when the SOC_{int} = SOC_{min}. Finally, Figs. 11 and 12 depict the optimal profiles of load power and the system voltage for the entire network. They show the optimal power required to be supplied from the utility grid and how stable the system voltage is. For the entire network, the results are assessed with SOC_{int}= [0.4, 0.9].

4.2. Discussion of the results

From Figs. 8–10, it is observed that the power from PV to supply the load is approximately the same for both linear control schemes. This is regardless of the value of SOC_{int}, as shown in Figs. 8(a), 9(a) and 10(a). The same pattern can also be captured when the solar power wants to charge the BESS, as depicted in Figs. 8(b), 9(b) and 10(b). However, the feedback strategy of the linear closed-loop scheme provides necessary information into the system, which consists of discharging the battery when there is any optimal capacity of BESS to be used. Figs. 8(f), 9(f) and 10(f) confirm this dynamic behaviour. An absolute difference was observed between the open and closed-loop schemes for energy from the BESS. The closed offers more into the opportunity energy, Figs. 8(d), 9(d) and 10(d), rather than the demand side. The first linear strategy tries to balance the sharing of the power from the BESS. The MPC strategy results differ from all linear models, and this quadratic

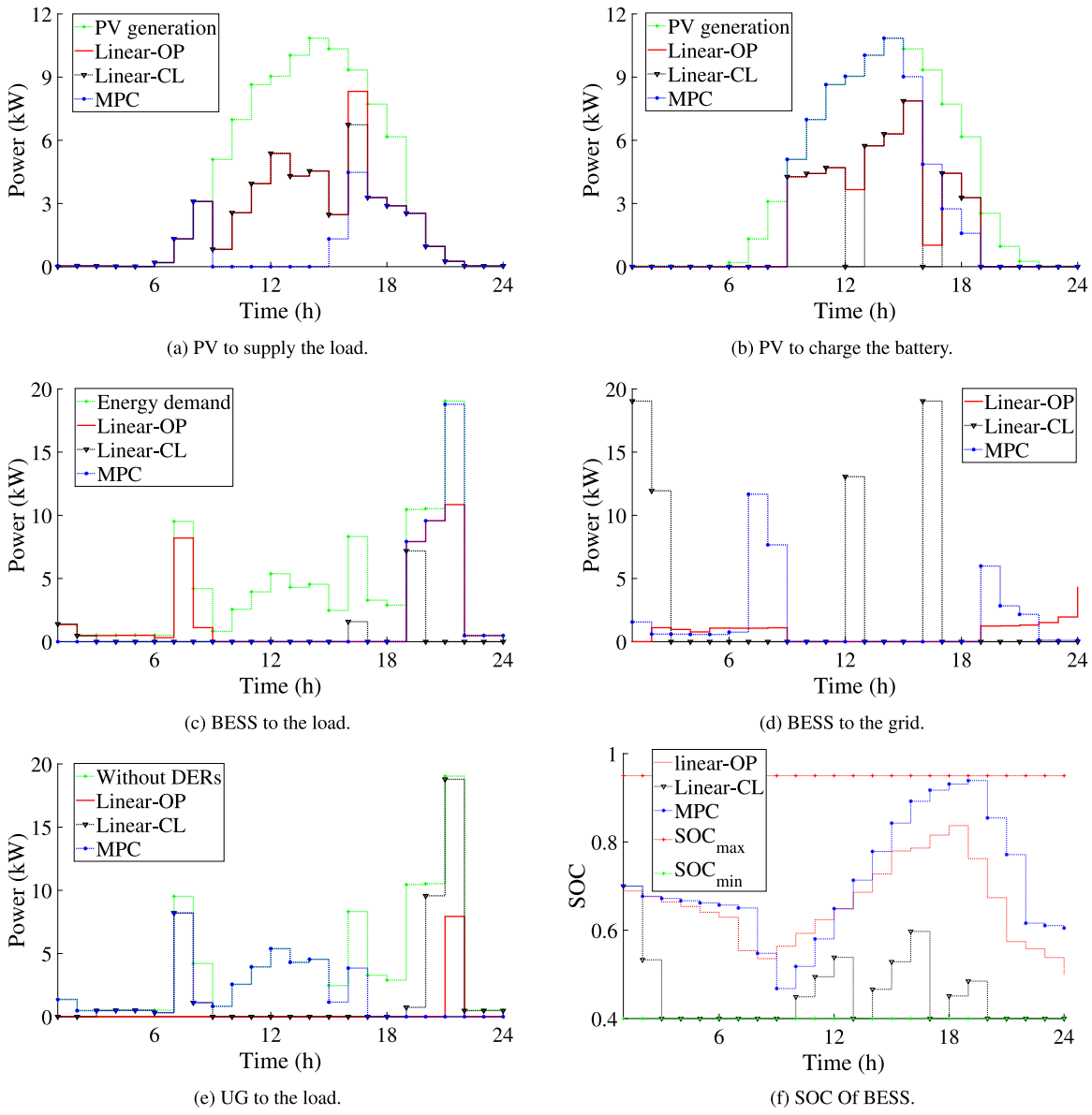

(a) PV to supply the load.

(b) PV to charge the battery.

(c) BESS to the load.

(d) BESS to the grid.

(e) UG to the load.

(f) SOC Of BESS.

Fig. 9. Optimum coordination of microgrid at bus 7, with initial SOC_{int} = 0.7.

computational scheme provides robust patterns that dynamically learn and effectively coordinate the system behaviour.

Figs. 8(e), 9(e) and 10(e) present the optimal results of the grid to feed the end-user. This profile compares the three control schemes with the optimal power from the utility without integrating DERs. BESS and PV systems also play an important role in minimising the power from the utility grid, as shown in Figs. 8–10. Thus, It could be challenging to select the most suitable strategy in the context of minimising the power from the utility grid within the selected SOC_{int} of the BESS. This is because it is observed that each system dynamic possesses its intrinsic computational behaviour regardless of the value of SOC_{int} to decide when to minimise the power from the utility grid.

Nevertheless, the robustness of the MPC demonstrates consistency in terms of minimising the energy from the utility grid and maximising the power flow in DEGs. Besides, the power from BESS to supply the load is optimally used to avoid fully discharging the battery in the MPC scheme, as demonstrated in Figs. 8(c), 9(c) and 10(c). In the closed-loop approach, the power from the BESS to the load slightly increases when the SOC_{int} increases. The same observation is made in the MPC scheme, as shown in Figs. 8–10. All models optimally provide different patterns, as presented in Figs. 8–12. The system constraint plays a major role in the optimal computational of each strategy. Besides, all developed schemes are robust in handling the system constraints presented in Section 3.5 and uncertainties from DERs, as illustrated in Figs. 8–10. Thus, $\forall t \in N \Rightarrow$ Eq. (4) and if $P_{pv}(t) = 0 \Leftrightarrow P_d = P_{dc} + P_{ug}$ is satisfied in all schemes.

It is challenging to discuss the tremendous impact of the pay-back energy on the closed-loop scheme compared to other developed methods, such as closed loop and MPC. This challenge is presented in Figs. 8(f), 9(f) and 10(f), where the BESS is maximally affected during the closed-loop process. Thus, the BESS is heavily featured in terms of the power injected into the grid. The impact of this control scheme can be more critical in terms of the end-users minimising energy consumption. However, in the context of the payback energy, it can be less valuable than having more injected power into the grid due to the significant reduction of the SOC. This is one of the reasons the opportunity energy is also considered in the economic performance indications, as formulated in Table 3.

Figs. 11 and 12 show the optimal power demand in the network. This total load demand of the network without the application of the

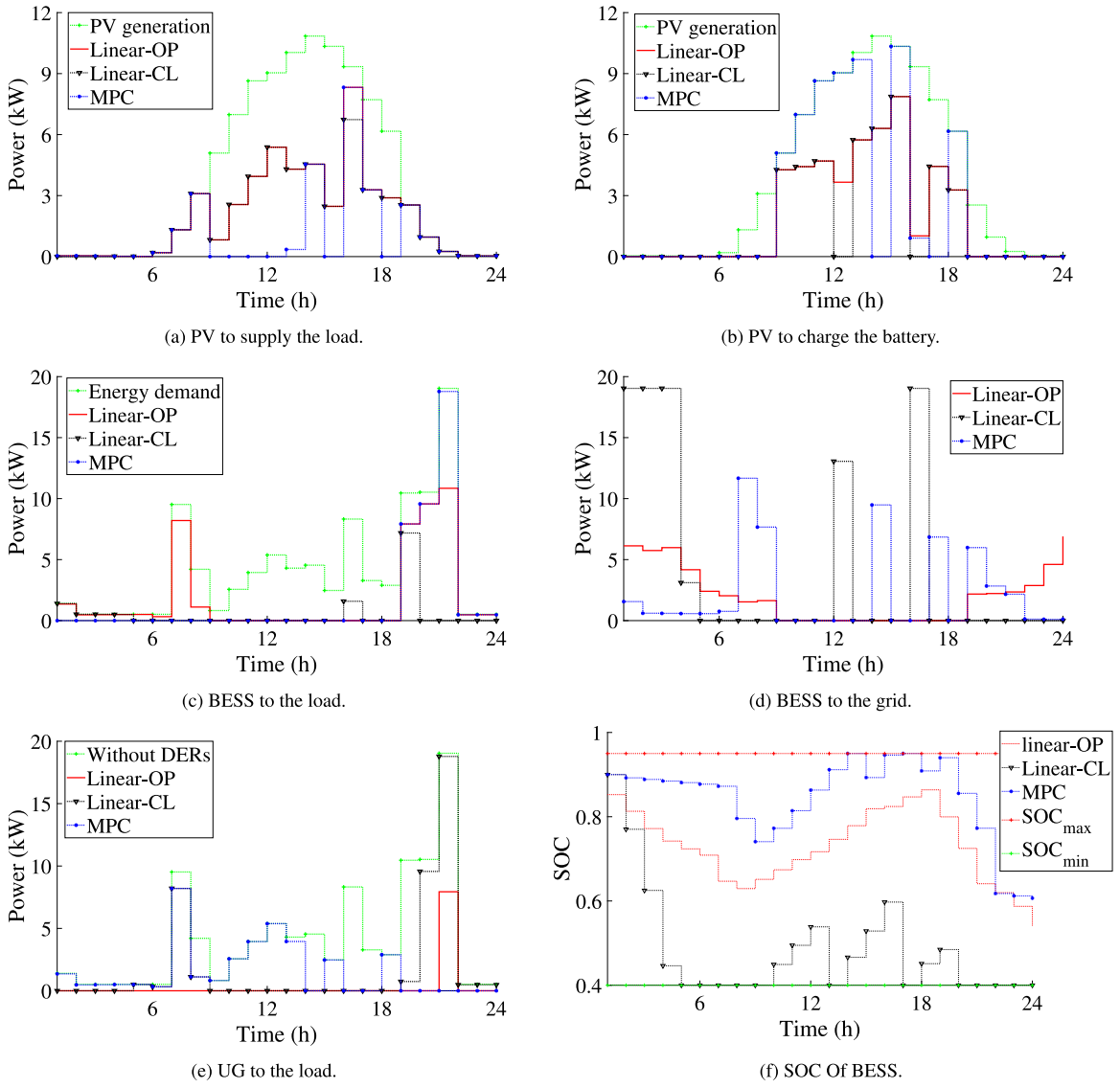

(a) PV to supply the load.

(b) PV to charge the battery.

(c) BESS to the load.

(d) BESS to the grid.

(e) UG to the load.

(f) SOC Of BESS.

Fig. 10. Optimum coordination of microgrid at bus 7, with initial SOC_{int} = 0.9.

Hs is presented in Fig. 7. It can be observed that the quantity of energy on the demand side has been minimising each strategy. Besides, the system voltage is within the acceptable value, as detailed in Figs. 11 and 12. Therefore, the suitability of the proposed models is of great value regardless of the selected value of the SOC_{int}. However, it is problematic to conclude this affirmation. Therefore, the KPIs' framework, as presented in Table 3, proceeds to evaluate the dynamic improvement of each strategy.

Table 6 provides the KPIs of the system implementation at bus 7. This analysis is developed using the model presented in Section 3.7 and the implementation assessment provided in Tables 4 and 5. Therefore, the system's performance in terms of economic viability, environmental impact, and user satisfaction are provided for the microgrid at bus 7. This assessment is an advanced analysis of KPIs for a suitable implementation and monitoring of microgrids, as described in Table 3. These KPIs are evaluated for each scenario by considering two initial SOCs of BESS and comparing them with some relevant published works. It has firstly been observed that most relevant published do not feel the inherent KPIs, as presented in Section 3.7. One of the particularities of this study is also the fact of introducing the breakdown cost (57).

In Table 6, it has been observed that the closed-loop scheme provides the best KPIs compared to other strategies. This is, nonetheless, the selected value of SOC_{int}. The open-loop scheme is the second. However, in terms of system robustness throughout the computational process of selecting SOC_{int}, when considering the ratio of SOC_{int} = 0.4 and 0.9, some critical economic KPIs, such as COE, CS, EPBT, NPV, ROI, and even some environment and operational KPIs, MPC scheme is reliable. The comparison of this work with some relevant published studies, as detailed in Table 6, details that some of the economic performances, including COE and LCOE, are higher than those that are being previously studied. Therefore, it has been observed that some previous works do not often consider certain rudimentary factors and parameters of the system implementation and partially assess the economic performance indicators of microgrids, as detailed in Section 3.7. The environmental and operational performance indicators of this study compared to the relevant published ones are acceptable for arguing that this work effectively addresses user satisfaction challenges

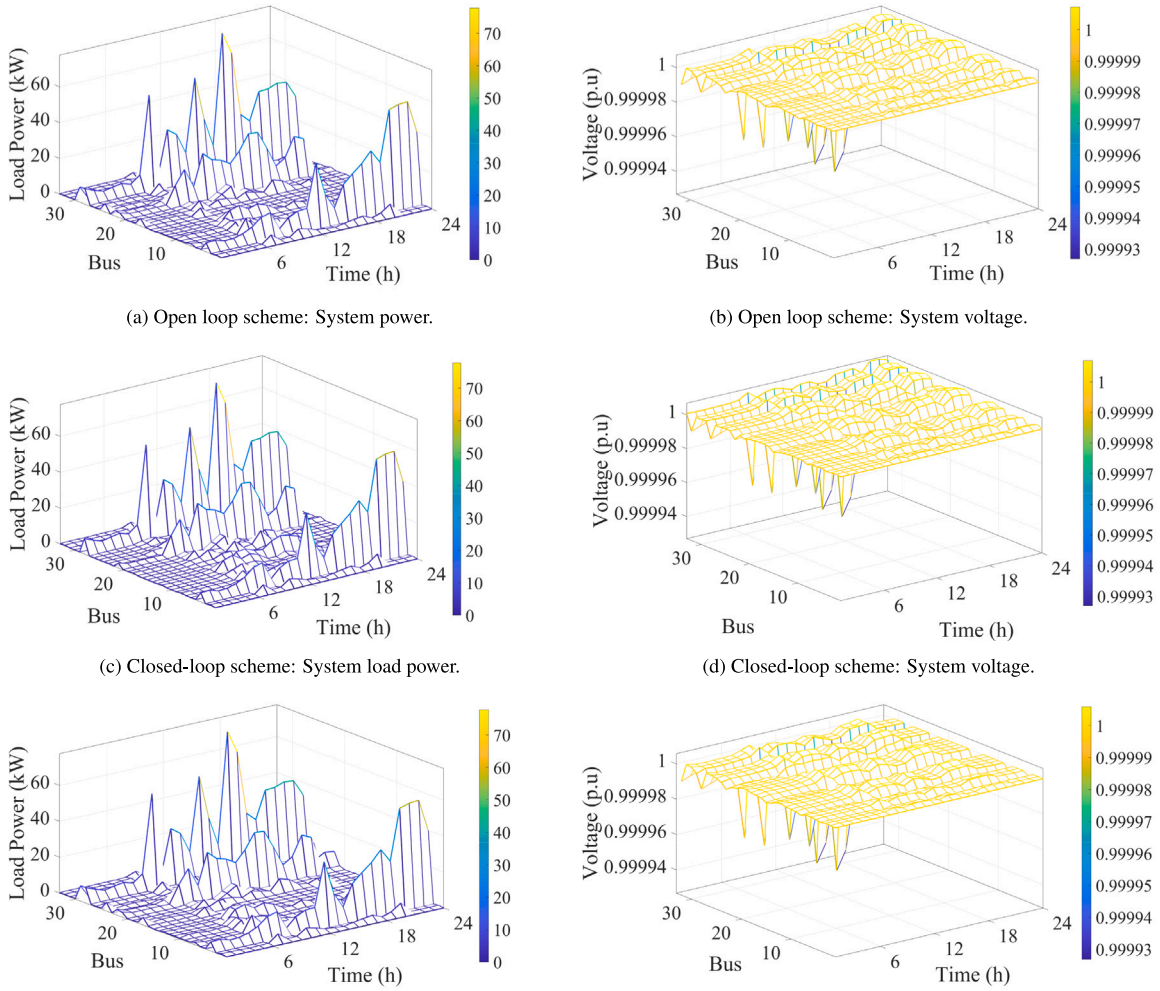

(a) Open loop scheme: System power.

(b) Open loop scheme: System voltage.

(c) Closed-loop scheme: System load power.

(d) Closed-loop scheme: System voltage.

(e) MPC scheme: System load power.

(f) MPC scheme: System voltage.

Fig. 11. Optimal network coordination, with $\text{Soc}_{int} = 0.4$.

and environmental impact. Besides, when benchmarking the KPIs with other studies, one of the concerns that can arise is all these works do not necessarily contain the same configuration, as presented in Figs. 1 and 2, including parameters and variables. Nonetheless, these economic, environmental and operational performance indicators are reliable and guarantee an effective energy trilemma.

The closed-loop scheme significantly offers several best KPIs, compared to the open-loop and MPC strategy, as presented in Table 6. However, the closed-loop method has a severe disadvantage in terms of the energy flow on the battery. This aims to sustain the stability and flexibility of the SH dynamic when tied to the grid. The difference depicted in Figs. 8(f), 9(f), and 10(f) can rescind all the advantages the power flow structure offers from the closed-loop model. The same issue can also be observed in the open-loop strategy and particularly in the MPC scheme when SOC_{int} is at its minimal value. The dynamic model of the battery is prominent in terms of the energy coordination of the SH. Therefore, these profiles demonstrate that the MPC strategy provides an excellent dynamic of BESS compared to other schemes. Besides, this advantage can also sustain all challenges of the unpredicted behaviour of DEGs and the effective coordination of the entire network, making the MPC model a more secure and reliable computational method for the efficiency of the energy market.

Table 7 evaluates the system saving of the entire network. This assessment is prosecuted against the total demand, as presented in Fig. 7. The results depicted in Figs. 11–12 play an important role in this analysis. Figs. 11–12 show that the difference in system voltage mostly depends on the power loss in the electrical network. There are three scenarios for the system voltage based on each computational scheme, including the open-loop model, the closed-loop scheme, and the MPC method. Regarding the system voltage constraints formulated in Eq. (40) and limits set between 0.9 and 1.1 per unit (p.u) with an initial value set of 1 p.u, it is observed, in Figs. 11(b), 11(d), 11(f), 12(b), 12(d) and 12(f) that the system voltage for the entire network for the computational developed models is at its acceptable operational range. Besides, as presented in Table 7, the decrease in the power loss is observed for both linear (open and closed-loop) and quadratic (MPC) models. Thus, from Figs. 11–12, the system constraints optimally handle any increase in the system voltage through the effectiveness of the developed coordination strategies. Therefore, an acceptable improvement of the system voltage is guaranteed when integrating SHs into the electrical network with a considerable amount of DEGs.

There is an energy-saving value ranging between [25.49, 36.14]% of the total power demand in the entire electrical network for the open-loop scheme. The same observation is made for linear closed-loop and MPC strategies, which provide a system energy saving of roughly [23.99, 25.9]% and [27.68, 28.41]%. As observed in Table 6, the MPC keeps providing robust rapport between the SOC_{int} value compared to linear strategies. This includes savings and active power loss, as shown in Table 7. One of the most important observations of the analysis is the deviation impact between both linear control structures. The

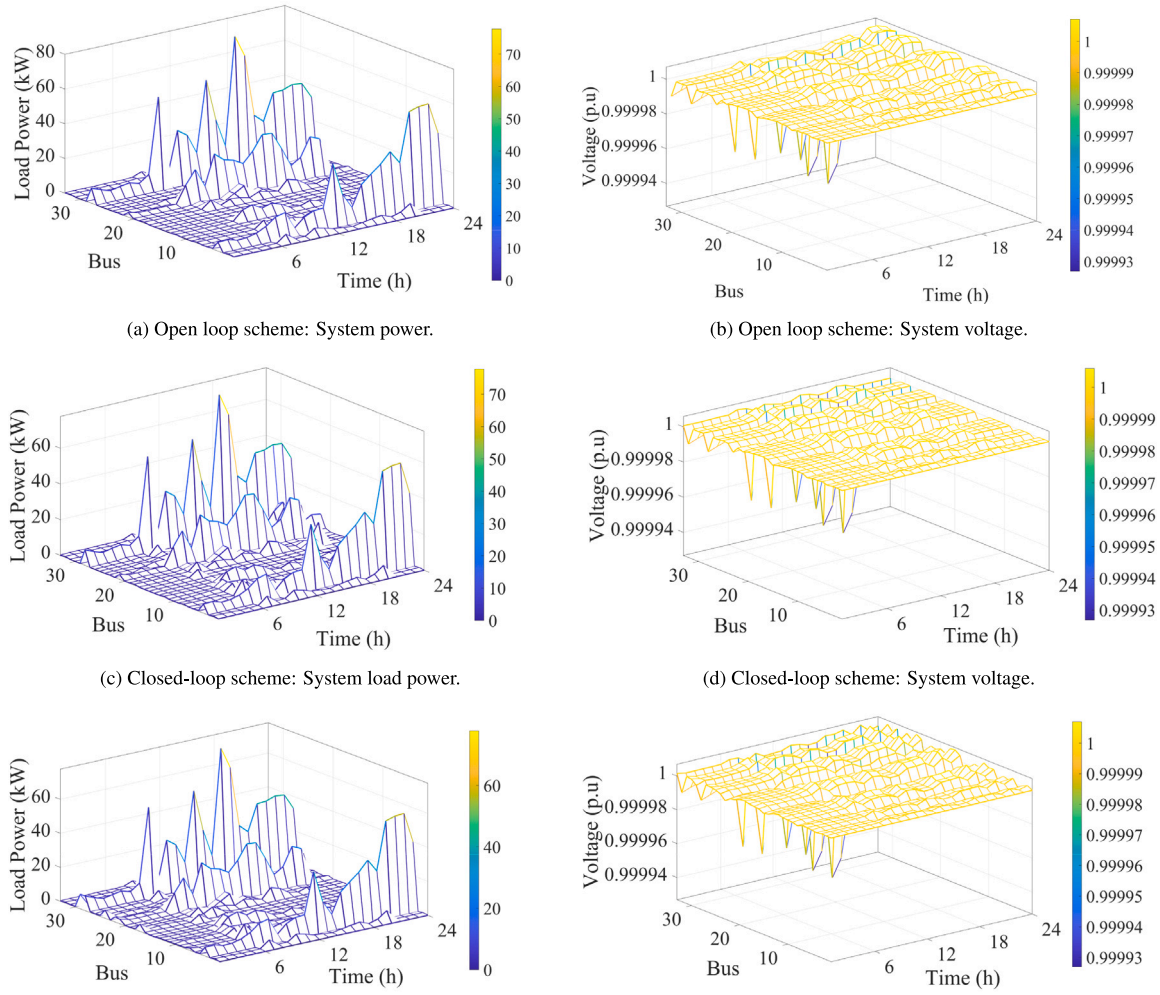

(a) Open loop scheme: System power.

(b) Open loop scheme: System voltage.

(c) Closed-loop scheme: System load power.

(d) Closed-loop scheme: System voltage.

(e) MPC scheme: System load power.

(f) MPC scheme: System voltage.

Fig. 12. Optimal network coordination, with $\text{Soc}_{int} = 0.9$.

Table 6
KPIs for energy coordination of microgrid: Performance assessment of the system design and benchmark against other existing methods.

Performance Indicators		Assessment at bus 7, with SOC_{int}= [0.40, 0.9]			Publish works: microgrid					
		Open Loop	Closed Loop	MPC	[62]	[65]	[12]	[66]	[67]	[68]
Economic	COE [$/kWh]	[0.391, 0.265]	[0.303, 0.207]	[0.362, 0.264]	0.071	–	–	–	–	0.0725
	CS [MM$]	[1.368, 2.410]	[1.481, 2.561]	[1.449, 1.962]	–	0.35	–	–	–	–
	EPBT [years]	[4.203, 2.387]	[3.885, 2.346]	[3.970, 2.932]	–	8	–	4-10.5	0.33–5.18	6.4
	LCOE [$/kWh]	[0.316, 0.316]	[0.329, 0.329]	[0.304, 0.290]	–	–	0.082–0.099	–	–	0.072-0.103
	NPV [MM$]	[0.546, 1.180]	[0.614, 1.2722]	[0.595, 0.907]	0.36	–	–	–	–	1.83
	ROI [%]	[375.81, 737.93]	[414.83, 790.41]	[403.76, 582.13]	–	–	–	–	–	–
Environ.	CER [Gg CO_2]	[0.383, 0.674]	[0.414, 0.717]	[0.405, 0.549]	–	–	–	–	–	0.19
	RF [%]	[80.67, 80.68]	[80.67, 80.68]	[80.68, 80.68]	–	–	–	–	–	31.1
	TCO_2E [Gg CO_2]	[0.100, 0.038]	[0.208, 0.195]	[0.116, 0.168]	0.823	–	–	–	–	0.865
Operat.	BU [%]	[18.18, 51.94]	[22.70, 57.78]	[26.25, 49.65]	–	–	–	–	–	–
	SCR [%]	[59.73, 59.73]	[57.72, 57.58]	[47.26, 31.82]	–	–	50–84	–	–	–
	SSR [%]	[48.19, 48.19]	[46.57, 46.45]	[38.13, 25.67]	–	–	50–76	–	88.21	-
Envrion.: Environmental		Operat.: Operational	Op.: Opportunity	Gg: gigagram	MM: million	N_{yr}: 20	Solar uncertainty: 15%			

deviation difference is about [1.95, 10.24]%, which is considerable for a system improvement comparison. For instance, in Fig. 12, a significant deviation between the open and closed-loop models can be observed. There is a considerable deviation of about [3.69, 2.50]% and [1.74, –7.73]% between the MPC scheme and the open-loop and closed-loop models.

The power-saving, as presented in Table 7, resulted from the power demand from the SHs, P_{ug_i} as presented in Eq. (4), without considering

Table 7
Power saving analysis, with SOC_{int} =[0.4, 0.9].

Scenarios	Consuming power (kW)	Saving power (kW)	Active power loss (kW)
Open Loop	[216.004, 1833.031]	[744.756, 1037.729]	[0.042216, 0.042177]
Closed Loop	[2182.00, 2127.00]	[688.76, 743.755]	[0.040619, 0.040598]
MPC	[2075.933, 2055.201]	[794.827, 815.559]	[0.041062, 0.041895]

In Fig. 7, the total power demand: 2870.76

the opportunity power generated from DEG-tied to the grid, P_{op_i}. Moreover, the system operates so that the DSO manages the injected power into the microgrid. As a result, the energy injected into the grid is also more valuable than the energy supplied to the SH from the utility grid, as depicted in Figs. 8(d), 9(d), and 10(d). Therefore, intelligent home systems offer a substantial payback energy cost to the end-users, which is detailed in Table 6. This is why the ROI of each strategy, regardless of SOC_{int} values, is over 350%, with suitable EPBT implementations varying between 2.3 to 4.2 years.

5. Conclusion

Dynamic power coordination of a smart microgrid using a DR program under real-time electricity pricing is framed to harmonise the energy flow of the electrical network. This strategy applies system analysis to formulate optimal MAS coordination with autonomous agents to guarantee cost reduction, energy savings, voltage stability, and power loss minimisation of microgrids based on a combination of EMS and OPF. Therefore, three optimal control schemes, including open-loop, closed-loop and MPC, are designed to orchestrate the dynamic behaviour of the system variables. A KPI framework is also introduced to validate the improvement of the design and the robustness of the developed approaches. It is observed that each developed strategy relatively provides the best performance indicators, such as EPBT of 2.38 to 4.20, 2.34 to 3.88, and 2.93 to 3.97 years for open-loop, closed-loop and MPC schemes, respectively, with more than 350% of ROI for an isolated SH. Besides, the closed-loop scheme performs better in terms of system performance, followed by the open-loop strategy, with several higher values of KPIs compared to MPC. However, MPC is robust in terms of system computational with stable values of KPIs regardless of the SOC_{int} of BESS. This is also observed in the energy flow from the BESS. Besides, the developed strategies demonstrate a suitable coordination approach to integrate MAs in the microgrid platform. Therefore, the developed open-loop, closed-loop and MPC approaches compute an excellent combined behaviour of the system dynamics that can ensure both payback energy and DER optimal power flow. The power saving range is between 23.99% to 36.14%. These savings are assessed regardless of the opportunity energy. Furthermore, all control strategies offer an acceptable voltage level in the electrical network, roughly 1 p.u in each developed optimal control scheme with minimal power loss of about 0.04 kW. Therefore, the developed dynamic coordination model demonstrates the effectiveness of each designed strategy in the context of energy management, KPI structure, power savings, voltage stability, and power loss minimisation. This work also provides an adequate scalability framework for an effective microgrid implementation.

Future research can focus on the synergy of the multi-energy system. The strategy will look at the multi-vector energy coordination system of a microgrid in which the integrated DR concept is introduced. This approach will aim to guarantee the energy trilemma of the entire system for an adequate energy market.

CRediT authorship contribution statement

Nsilulu T. Mbungu: Writing – review & editing, Writing – original draft, Visualization, Validation, Supervision, Software, Resources, Project administration, Methodology, Investigation, Funding acquisition, Formal analysis, Data curation, Conceptualization. **Mukwanga W. Siti:** Writing – review & editing, Writing – original draft, Visualization, Validation, Supervision, Resources, Methodology, Investigation, Formal analysis, Data curation, Conceptualization. **Ramesh C. Bansal:** Writing – review & editing, Validation, Supervision, Methodology, Investigation, Funding acquisition, Formal analysis. **Raj M. Naidoo:** Writing – review & editing, Visualization, Validation, Supervision, Methodology, Investigation, Funding acquisition, Conceptualization. **A. Elnady:** Writing – review & editing, Visualization, Validation, Software, Methodology, Investigation, Funding acquisition, Formal analysis. **Ali A. Adam Ismail:** Writing – review & editing, Visualization, Validation, Methodology, Investigation, Funding acquisition, Formal analysis. **Ahmed G. Abokhali:** Writing – review & editing, Visualization, Validation, Methodology, Investigation, Funding acquisition, Formal analysis. **Abdul-Kadir Hamid:** Writing – review & editing, Visualization, Validation, Methodology, Investigation, Funding acquisition, Formal analysis.

Declaration of competing interest

The authors declare that they have no known competing financial interests or personal relationships that could have appeared to influence the work reported in this paper.

Data availability

Data will be made available on request.

References

[1] Marot A, Kelly A, Naglic M, Barbesant V, Cremer J, Stefanov A, et al. Perspectives on future power system control centers for energy transition. J Mod Power Syst Clean Energy 2022;10(2):328–44.
[2] Kamwa I. Grid digital transition: Operating the smart grid in a digital world [editor's voice]. IEEE Power Energy Mag 2024;22(3):4–14.
[3] Gaspar J, Cruz T, Lam C-T, Simões P. Smart substation communications and cybersecurity: A comprehensive survey. IEEE Commun Surv Tutor 2023;25(4):2456–93.
[4] Hussain I, Ali S, Khan B, Ullah Z, Mehmood C, Jawad M, et al. Stochastic wind energy management model within smart grid framework: a joint bi-directional service level agreement (SLA) between smart grid and wind energy district prosumers. Renew Energy 2019;134:1017–33.
[5] Babayomi O, Zhang Z, Dragicevic T, Hu J, Rodriguez J. Smart grid evolution: Predictive control of distributed energy resources—A review. Int J Electr Power Energy Syst 2023;147:108812.
[6] Ahsan F, Dana NH, Sarker SK, Li L, Muyeen S, Ali MF, et al. Data-driven next-generation smart grid towards sustainable energy evolution: techniques and technology review. Protect Control Mod Power Syst 2023;8(3):1–42.
[7] Mbungu NT, Ismail AA, AlShabi M, Bansal RC, Elnady A, Hamid AK. Control and estimation techniques applied to smart microgrids: A review. Renew Sustain Energy Rev 2023;179:113251.
[8] Karandeh R, Davoudi M, Cecchi V. Distributed control of behind-the-meter energy resources for multiple services. IEEE Trans Power Deliv 2021;37(3):2050–9.
[9] Ayub S, Ayob SM, Tan CW, Taimoor M, Ayub L, Bukar AL, et al. Analysis of energy management schemes for renewable-energy-based smart homes against the backdrop of COVID-19. Sustain Energy Technol Assess 2022;52:102136.
[10] Siano P, Cecati C, Yu H, Kolbusz J. Real time operation of smart grids via FCN networks and optimal power flow. IEEE Trans Ind Inform 2012;8(4):944–52.
[11] Li S, Zhu J, Dong H, Zhu H, Luo F, Borghetti A. Multi-time-scale energy management of renewable microgrids considering grid-friendly interaction. Appl Energy 2024;367:123428.
[12] Hernández J, Sanchez-Sutil F, Muñoz-Rodríguez F, Baier C. Optimal sizing and management strategy for PV household-prosumers with self-consumption/sufficiency enhancement and provision of frequency containment reserve. Appl Energy 2020;277:115529.

[13] Khan MW, Li G, Wang K, Numan M, Xiong L, Khan MA. Optimal control and communication strategies in multi-energy generation grid. IEEE Commun Surv Tutor 2023.
[14] Aktas A, Erhan K, Özdemir S, Özdemir E. Dynamic energy management for photovoltaic power system including hybrid energy storage in smart grid applications. Energy 2018;162:72–82.
[15] Achour Y, Ouammi A, Zejli D. Model predictive control based demand response scheme for peak demand reduction in a smart campus integrated microgrid. IEEE Access 2021;9:162765–78.
[16] Khan B, Shafiq S, Al-Awami AT. Artificial-neural-network-based autonomous demand response controller for thermostatically controlled loads. IEEE Syst J 2023.
[17] Said D. A survey on information communication technologies in modern demand side management for smart grids: Challenges, solutions, and opportunities. IEEE Eng Manag Rev 2022.
[18] Wen L, Zhou K, Feng W, Yang S. Demand side management in smart grid: A dynamic-price-based demand response model. IEEE Trans Eng Manag 2022.
[19] Muratori M, Rizzoni G. Residential demand response: Dynamic energy management and time-varying electricity pricing. IEEE Trans Power Syst 2015;31(2):1108–17.
[20] Alam MR, St-Hilaire M, Kunz T. Peer-to-peer energy trading among smart homes. Appl Energy 2019;238:1434–43.
[21] Arasteh F, Riahy GH. MPC-based approach for online demand side and storage system management in market based wind integrated power systems. Int J Electr Power Energy Syst 2019;106:124–37.
[22] Aminlou A, Mohammadi-Ivatloo B, Zare K, Razzaghi R, Anvari-Moghaddam A. Activating demand side flexibility market in a fully decentralized P2p transactive energy trading framework using ADMM algorithm. Sustainable Cities Soc 2024;100:105021.
[23] Clift DH, Hasan KN, Rosengarten G. Peer-to-peer energy trading for demand response of residential smart electric storage water heaters. Appl Energy 2024;353:122182.
[24] Mbungu NT, Bansal RC, Naidoo RM, Siti MM, Ismail AA, Elnady A, et al. Performance analysis of different control models for smart demand–supply energy management system. J Energy Storage 2024;90:111809.
[25] Han J, Choi C-S, Park W-K, Lee I, Kim S-H. Smart home energy management system including renewable energy based on ZigBee and PLC. IEEE Trans Consum Electron 2014;60(2):198–202.
[26] Bertolini M, D'Alpaos C, Moretto M. Do smart grids boost investments in domestic PV plants? Evidence from the Italian electricity market. Energy 2018;149:890–902.
[27] Shil SK, Sadaoui S. Meeting peak electricity demand through combinatorial reverse auctioning of renewable energy. J Mod Power Syst Clean Energy 2018;6(1):73–84.
[28] Sharma M, Dhundhara S, Sran RS. Impact of hybrid electrical energy storage system on realistic deregulated power system having large-scale renewable generation. Sustain Energy Technol Assess 2023;56:103025.
[29] Wu J, Yang F. A dual-driven predictive control for photovoltaic-diesel microgrid secondary frequency regulation. Appl Energy 2023;334:120652.
[30] Zhao Z, Xu J, Guo J, Ni Q, Chen B, Lai LL. Robust energy management for multi-microgrids based on distributed dynamic tube model predictive control. IEEE Trans Smart Grid 2024;15(1):203–17.
[31] He H, Wang Y, Han R, Han M, Bai Y, Liu Q. An improved MPC-based energy management strategy for hybrid vehicles using V2V and V2I communications. Energy 2021;225:120273.
[32] Vásquez LOP, Redondo JL, Hervás JDÁ, Ramírez VM, Torres JL. Balancing CO2 emissions and economic cost in a microgrid through an energy management system using MPC and multi-objective optimization. Appl Energy 2023;347:120998.
[33] Arroyo J, Manna C, Spiessens F, Helsen L. Reinforced model predictive control (RL-MPC) for building energy management. Appl Energy 2022;309:118346.
[34] Xing X, Xie L, Meng H. Cooperative energy management optimization based on distributed MPC in grid-connected microgrids community. Int J Electr Power Energy Syst 2019;107:186–99.
[35] Klaimi J, Rahim-Amoud R, Merghem-Boulahia L, Jrad A. A novel loss-based energy management approach for smart grids using multi-agent systems and intelligent storage systems. Sustain Cities Soc 2018;39:344–57.
[36] Zhao T, Li Z, Ding Z. Consensus-based distributed optimal energy management with less communication in a microgrid. IEEE Trans Ind Inform 2018;15(6):3356–67.
[37] Kumar K, Bae S. Two-layer energy management strategy for renewable power-to-gas system-based microgrids. J Energy Storage 2023;61:106723.
[38] Neis P, Wehrmeister MA, Mendes MF, Pesente JR. Applying a model-driven approach to the development of power plant SCADA/EMS software. Int J Electr Power Energy Syst 2023;153:109336.
[39] Fattaheian-Dehkordi S, Tavakkoli M, Abbaspour A, Fotuhi-Firuzabad M, Lehtonen M. An incentive-based mechanism to alleviate active power congestion in a multi-agent distribution system. IEEE Trans Smart Grid 2020.
[40] Bian Y, Xie L, Ye J, Ma L, Cui C. Peer-to-peer energy sharing model considering multi-objective optimal allocation of shared energy storage in a multi-microgrid system. Energy 2024;288:129864.
[41] Menghwar M, Yan J, Chi Y, Amin MA, Liu Y. A market-based real-time algorithm for congestion alleviation incorporating EV demand response in active distribution networks. Appl Energy 2024;356:122426.
[42] Nawaz A, Wu J, Ye J, Dong Y, Long C. Distributed MPC-based energy scheduling for islanded multi-microgrid considering battery degradation and cyclic life deterioration. Appl Energy 2023;329:120168.
[43] Santos G, Morais H, Pinto T, Corchado JM, Vale Z. Intelligent energy systems ontology to support markets and power systems co-simulation interoperability. Energy Convers Manag: X 2023;20:100495.
[44] Mediwaththe CP, Blackhall L. Network-aware demand-side management framework with a community energy storage system considering voltage constraints. IEEE Trans Power Syst 2020;36(2):1229–38.
[45] Xu J, Fu H, Liao S, Xie B, Ke D, Sun Y, et al. Demand-side management based on model predictive control in distribution network for smoothing distributed photovoltaic power fluctuations. J Mod Power Syst Clean Energy 2022;10(5):1326–36.
[46] Yin S, Ai Q, Li J, Li D, Guo Q. Trading mode design for a virtual power plant based on main-side consortium blockchains. Appl Energy 2022;325:119932.
[47] Quijano DA, Padilha-Feltrin A, Catalão JP. Probabilistic rolling-optimization control for coordinating the operation of electric springs in microgrids with renewable distributed generation. IEEE Trans Sustain Energy 2022;13(4):2159–71.
[48] Jendoubi I, Sheshyekani K, Dagdougui H. Aggregation and optimal management of TCLs for frequency and voltage control of a microgrid. IEEE Trans Power Deliv 2020;36(4):2085–96.
[49] Gomez-Gonzalez M, Hernandez JC, Vera D, Jurado F. Optimal sizing and power schedule in PV household-prosumers for improving PV self-consumption and providing frequency containment reserve. Energy 2020;191:116554.
[50] Khawaja Y, Allahham A, Giaouris D, Patsios C, Walker S, Qiqieh I. An integrated framework for sizing and energy management of hybrid energy systems using finite automata. Appl Energy 2019;250:257–72.
[51] Zhu X, Wang J, Lu N, Samaan N, Huang R, Ke X. A hierarchical VLSM-based demand response strategy for coordinative voltage control between transmission and distribution systems. IEEE Trans Smart Grid 2019;10(5):4838–47.
[52] Mazidi M, Malakhatka E, Steen D, Wallbaum H. Real-time rolling-horizon energy management of public laundries: A case study in HSB living lab. Energy Convers Manag: X 2023;20:100462.
[53] Olival P, Madureira AG, Matos M. Advanced voltage control for smart microgrids using distributed energy resources. Electr Power Syst Res 2017;146:132–40.
[54] Zahedi R, Ahmadian A, SedghiSigarchi K, Gadh R. An optimal methodology for mitigating the impacts of EVs and solar systems on the grid by utilizing existing residential battery storage capacity with no further grid upgrades. In: 2023 IEEE transportation electrification conference & expo. ITEC, IEEE; 2023, p. 1–5.
[55] Kou X, Li F, Dong J, Starke M, Munk J, Xue Y, et al. A scalable and distributed algorithm for managing residential demand response programs using alternating direction method of multipliers (ADMM). IEEE Trans Smart Grid 2020;11(6):4871–82.
[56] Nguyen DT, Nguyen HT, Le LB. Dynamic pricing design for demand response integration in power distribution networks. IEEE Trans Power Syst 2016;31(5):3457–72.
[57] Kotsalos K, Marques L, Sampaio G, Pereira J, Gouveia C, Teixeira H, et al. On the development of a framework for the advanced monitoring of LV grids. In: IEEE on international conference on smart energy systems and technologies. SEST, Porto, Portugal; 2019, p. 1–6.
[58] Richardson I, Thomson M, Infield D, Clifford C. Domestic electricity use: A high-resolution energy demand model. Energy Build 2010;42(10):1878–87.
[59] Brunton SL, Kutz JN. Data-driven science and engineering: Machine learning, dynamical systems, and control. Cambridge University Press; 2022.
[60] Mbungu NT, Bansal RC, Naidoo RM, Bettayeb M, Siti MW, Bipath M. A dynamic energy management system using smart metering. Appl Energy 2020;280:115990.
[61] Kusakana K. Optimal peer-to-peer energy sharing between grid-connected prosumers with different demand profiles and renewable energy sources. IET Smart Grid 2021;4(3):270–83.
[62] Adefarati T, Bansal R, Naidoo R, Onaolapo K, Bettayeb M, Olulope P, et al. Design and techno-economic assessment of a standalone photovoltaic-diesel-battery hybrid energy system for electrification of rural areas: A step towards sustainable development. Renew Energy 2024;227:120556.
[63] Solarcoza. Solar battery comparison: Residential edition 2023. 2023, URL https://solar.co.za/solar-battery-comparison-residential-edition-2023, Accessed: 2024-07-25.
[64] Keck F, Lenzen M, Vassallo A, Li M. The impact of battery energy storage for renewable energy power grids in Australia. Energy 2019;173:647–57.
[65] Bokopane L, Kusakana K, Vermaak H, Hohne A. Optimal power dispatching for a grid-connected electric vehicle charging station microgrid with renewable energy, battery storage and peer-to-peer energy sharing. J Energy Storage 2024;96:112435.
[66] Jose JK, Sindhu M, Mohan V, Thomas V. Techno-economic analysis of decentralized residential microgrid with optimal prosumer selection. IEEE Access 2024;12:65403–17.

[67] Liu L, Liu W, Yao J, Jia T, Zhao Y, Dai Y. Life cycle energy, economic, and environmental analysis for the direct-expansion photovoltaic-thermal heat pump system in China. J Clean Prod 2024;434:139730.

[68] Shamim MMH, Silmee SM, Sikder MM. Optimization and cost-benefit analysis of a grid-connected solar photovoltaic system. AIMS Energy 2022;10(3).